IMMUNOLOGY

Magnitude and kinetics of the human immune cell response associated with severe dengue progression by single-cell proteomics

Makeda L. Robinson[1]†, David R. Glass[2]†‡, Veronica Duran[1,3], Olga Lucia Agudelo Rojas[4], Ana Maria Sanz[4], Monika Consuegra[5], Malaya Kumar Sahoo[2], Felix J. Hartmann[2]§, Marc Bosse[2], Rosa Margarita Gelvez[5], Nathalia Bueno[5], Benjamin A. Pinsky[1,2], Jose G. Montoya[6], Holden Maecker[7], Maria Isabel Estupiñan Cardenas[5], Luis Angel Villar Centeno[5], Elsa Marina Rojas Garrido[5], Fernando Rosso[4,8], Sean C. Bendall[2]†, Shirit Einav[1,3,7]*†

Approximately 5 million dengue virus–infected patients progress to a potentially life-threatening severe dengue (SD) infection annually. To identify the immune features and temporal dynamics underlying SD progression, we performed deep immune profiling by mass cytometry of PBMCs collected longitudinally from SD progressors (SDp) and uncomplicated dengue (D) patients. While D is characterized by early activation of innate immune responses, in SDp there is rapid expansion and activation of IgG-secreting plasma cells and memory and regulatory T cells. Concurrently, SDp, particularly children, demonstrate increased proinflammatory NK cells, inadequate expansion of CD16$^+$ monocytes, and high expression of the FcγR CD64 on myeloid cells, yet a signature of diminished antigen presentation. Syndrome-specific determinants include suppressed dendritic cell abundance in shock/hemorrhage versus enriched plasma cell expansion in organ impairment. This study reveals uncoordinated immune responses in SDp and provides insights into SD pathogenesis in humans with potential implications for prediction and treatment.

INTRODUCTION

Dengue virus (DENV) is a major threat to global health, infecting approximately 400 million people annually in over 130 countries (*1*, *2*). Each year, 3 million to 6 million symptomatic dengue patients develop severe dengue (SD) within days of symptom onset, which can be life-threatening (*2*–*4*). To identify patients at risk for SD progression, the World Health Organization (WHO) defined clinical criteria that distinguish dengue patients with warning signs (DWS) from those with uncomplicated dengue (D) and recommended their close monitoring (*2*). Nevertheless, since warning signs for SD often develop late in the course of illness and are nonspecific, their implementation does not capture all SD progressors (SDp) and has increased hospital care burden (*5*–*7*). While we and others have recently identified candidate clinically usable biomarkers for early identification of SDp (*7*–*10*), additional validation is ongoing and novel biomarkers are needed.

The best characterized risk factor for SD is secondary infection with a heterologous DENV serotype causing antibody-dependent enhancement (ADE) of infection (*11*–*13*). Additional factors, including increased plasma cells (*14*, *15*), aberrant T cell responses (*16*), cytokine storm (*16*, *17*), and high and prolonged viremia, have been implicated in the development of SD (*18*, *19*). However, since our understanding of SD pathogenesis is largely based on cultured cells and immunocompromised mouse studies, the role of these and other factors in natural infection in humans is poorly characterized. Moreover, it remains unknown how age affects the outcome of DENV infection—with some studies showing greater risk of SD progression in children and others in adults (*20*–*23*)—or why SD manifests as dengue hemorrhagic fever (DHF) and dengue shock syndrome (DSS) in some but as organ impairment (OI) in others (*2*).

To address these gaps in knowledge, we applied mass cytometry [cytometry by time of flight (CyTOF)], a proteomic single-cell approach, to 124 peripheral blood mononuclear cell (PBMC) samples from our dengue Colombia cohort. The unique design and clinical heterogeneity of our cohort facilitated comprehensive analysis of immune cell subtype abundance and functional marker expression revealing distinct and overlapping responses between (i) SDp and non-progressors, (ii) SDp adults and children, and (iii) SDp who manifested with DHF/DSS or OI. Longitudinal sample analysis profiled the kinetics of the immune response starting before progression to SD through convalescence, revealing dysregulation of the temporal switch between innate and adaptive immune responses associated with early exuberant immune regulation in SDp.

[1]Division of Infectious Diseases and Geographic Medicine, Department of Medicine, Stanford University School of Medicine, Stanford, CA, USA. [2]Department of Pathology, Stanford University School of Medicine, Stanford, CA, USA. [3]Chan Zuckerberg Biohub, 499 Illinois St., 4th Floor, San Francisco, CA 94158, USA. [4]Clinical Research Center, Fundación Valle del Lili, Cali, Colombia. [5]Centro de Atención y Diagnóstico de Enfermedades Infecciosas (CDI), Fundación INFOVIDA, Bucaramanga, Colombia. [6]Palo Alto Medical Foundation, Dr. Jack S. Remington Laboratory for Specialty Diagnostics, Palo Alto, CA, USA. [7]Department of Microbiology and Immunology, Stanford University School of Medicine, Stanford, CA, USA. [8]Department of Internal Medicine, Division of Infectious Diseases, Fundación Valle del Lili, Cali, Colombia.
*Corresponding author. Email: seinav@stanford.edu
†These authors contributed equally to this work.
‡Present address: Vaccine and Infectious Diseases Division, Fred Hutchinson Cancer Center, Seattle, WA, USA.
§Present address: Systems Immunology and Single-Cell Biology, German Cancer Research Center (DKFZ), Heidelberg, Germany.

RESULTS

High-dimensional immune profiling delineates disease severity in dengue infection

While orchestrating protection from DENV upon infection, a dysregulated immune response is thought to contribute to SD pathogenesis. To broadly profile the individual components of the immune response against DENV infection and to comprehensively understand the complex interplay that dictates disease severity, we collected longitudinal PBMC and serum samples from adults and children enrolled in the dengue Colombia cohort and performed CyTOF analysis. We used an antibody panel targeting 36 cellular markers encompassing proteins for cell type identification, immune activation, immune checkpoint, and Fc binding. We performed CyTOF analysis on a total of 124 samples from healthy controls C ($n = 15$), D ($n = 40$), DWS ($n = 23$), and SDp ($n = 22$) patients of whom 19 progressed to SD within several days following enrollment and 3 met criteria of SD at presentation (Fig. 1A and tables S1.1, S1.2, and S1.3). The first sample from all patients was obtained within 0 to 10 days following fever onset, designated acute infection, with a median of 5 days in all disease categories (table S1.3). Additional samples obtained from some patients during the acute phase and following recovery, designated convalescence, were also included, albeit only in longitudinal analyses. Most patients were previously exposed to DENV (see Materials and Methods), as expected for an endemic region (fig. S1A and table S1.3).

Following singlet gating, normalization, and quality filtering (fig. S1, B to D), the full dataset consisted of 9,051,718 cells. To capture patterns of cell abundance and protein expression at different levels of granularity, we clustered cells at three resolutions: 4 cell types [B, natural killer (NK), myeloid, and T cells] (Fig. 1B, panels), 11 cell subtypes (Fig. 1C, colors), and 29 cell populations (Fig. 1B, individual rows). We used expression of lineage-specific proteins (Fig. 1B, columns) to cluster cells into predefined immune cell subtypes so that differential expression of activation, checkpoint, and Fc-binding proteins would not bias clustering (see Materials and Methods). Differential abundance of immune cell phenotypes was evident by Uniform Manifold Approximation and Projection (UMAP) analysis (*24*) of the entire cohort (Fig. 1C) and the various disease severity categories (fig. S1E), regardless of cluster labels.

To quantitatively capture the state of the immune system, we compiled a set of 378 features consisting of cell population abundances and mean expression values for each sample (Fig. 1D). With this feature set, we performed pairwise distribution tests to identify features significantly different between severity categories in the setting of acute infection (within 10 days of fever onset) (table S2), convalescence (table S3), adults and children (table S4), SD categories (table S5) (Fig. 1D), and early acute time points (within 8 days of infection) (table S6).

To compare immune features between disease severity categories, we compiled samples collected within 10 days after reported symptom onset. When several samples were available, we used only the earliest sample to enrich for acute infection and avoid bias from overrepresentation of any single patient. For all features, we performed pairwise Wilcoxon rank sum tests between disease categories, corrected for multiple hypotheses [false discovery rate (FDR) method], and quantified effect sizes (table S2). Linear discriminant analysis (LDA) (*25*) using all features that were significantly different between any two severity categories ($q < 0.05$ and $|\text{effect size}| > 0.5$) effectively separated the dengue severity categories (Fig. 1E), confirming that our analytic framework captured substantial differences in the immune state.

To visualize differences in cell population abundances between SDp and D patients, we plotted the $\log_2$ SDp/D ratio of median abundances (% of $CD45^+$ cells) (Fig. 1F). The abundance of plasma cells ($q = 0.003$) and regulatory T cells (T_{regs}) ($q = 0.025$) was significantly greater in SDp than in D patients. In contrast, the abundance of $CD16^+$ monocytes ($q = 0.002$) and $CD8^+$ T effector memory cells reexpressing CD45RA (EMRA) associated with cellular senescence and terminal differentiation (*26*) was significantly lower in SDp than in D ($q = 0.018$). Trends toward expansion of conventional type 1 dendritic cells [cDC1s; stimulate $CD8^+$ T cell responses by cross-presentation (*27*)] and plasmacytoid dendritic cells [pDCs; type I interferon (IFN) producing (*28*)], concurrent with a reduction of cDC2s [predominately prime $CD4^+$ T cells (*29*) and $CD4^+$ TEMRAs in SDp relative to D], were also observed. Together, these results demonstrate that our experimental and analytical approaches capture differences in immune cell subtype abundance with differential disease severity during the acute phase of DENV infection.

Immune activation and regulation are simultaneously enriched in SDp

Since plasma cells were more abundant in SDp patients, we compared their abundance across all disease severity categories. While lower than SDp, D patients had significantly higher plasma cell abundance than C ($q = 0.027$), as expected during an acute viral infection (Fig. 2A). Nonetheless, SDp had higher plasma cell abundance (median = 7.64%) than DWS (median = 1.85%, $q = 0.044$), D (median = 1.44%, $q = 0.003$), and C subjects (median = 0.40%, $q = 0.00006$). Class-switched plasma cells in SDp were enriched for immunoglobulin G (IgG) over IgA ($q = 0.040$) (Fig. 2B) and expressed greater levels of Ki-67 relative to D ($q = 0.005$) (Fig. 2C), indicating greater production of the antibody isotype associated with ADE (*30*) and cell proliferation, respectively. Plasma cell abundance and plasma cell IgG usage diminished in both D and SDp in convalescent samples (fig. S2, A and B). Mean Ki-67 expression in plasma cells in SDp remained high in convalescence and, in D, was significantly increased in convalescent samples over acute samples ($P = 0.0002$) (Fig. 2D). These convalescent expression patterns contrast expression in C (Fig. 2C), suggesting that DENV infection induced heightened plasma cell activation even weeks to months after acute infection.

Next, we asked whether increased immune cell proliferation and activation was a common feature of SD progression. Thirteen of 29 cell subtypes, encompassing B, T, NK, and myeloid cell populations, had higher mean Ki-67 expression in acute SDp than D samples ($q < 0.05$) (Fig. 2E). These trends held when quantifying Ki-67 percent positivity (fig. S2C). Moreover, the mean expression of the general activation marker CD38, which is involved in cell adhesion, migration, and signal transduction, among others (*31*), was higher in SDp than in D in 14 of 29 cell subtypes ($q < 0.05$), confirming the greater activation of multiple cell populations via an orthogonal measurement (fig. S2D). The differences in Ki-67 and CD38 expression largely resolved at convalescence, although plasma cells and T_{regs} maintained the highest median Ki-67 expression levels in both SDp and D patients (fig. S2, E and F).

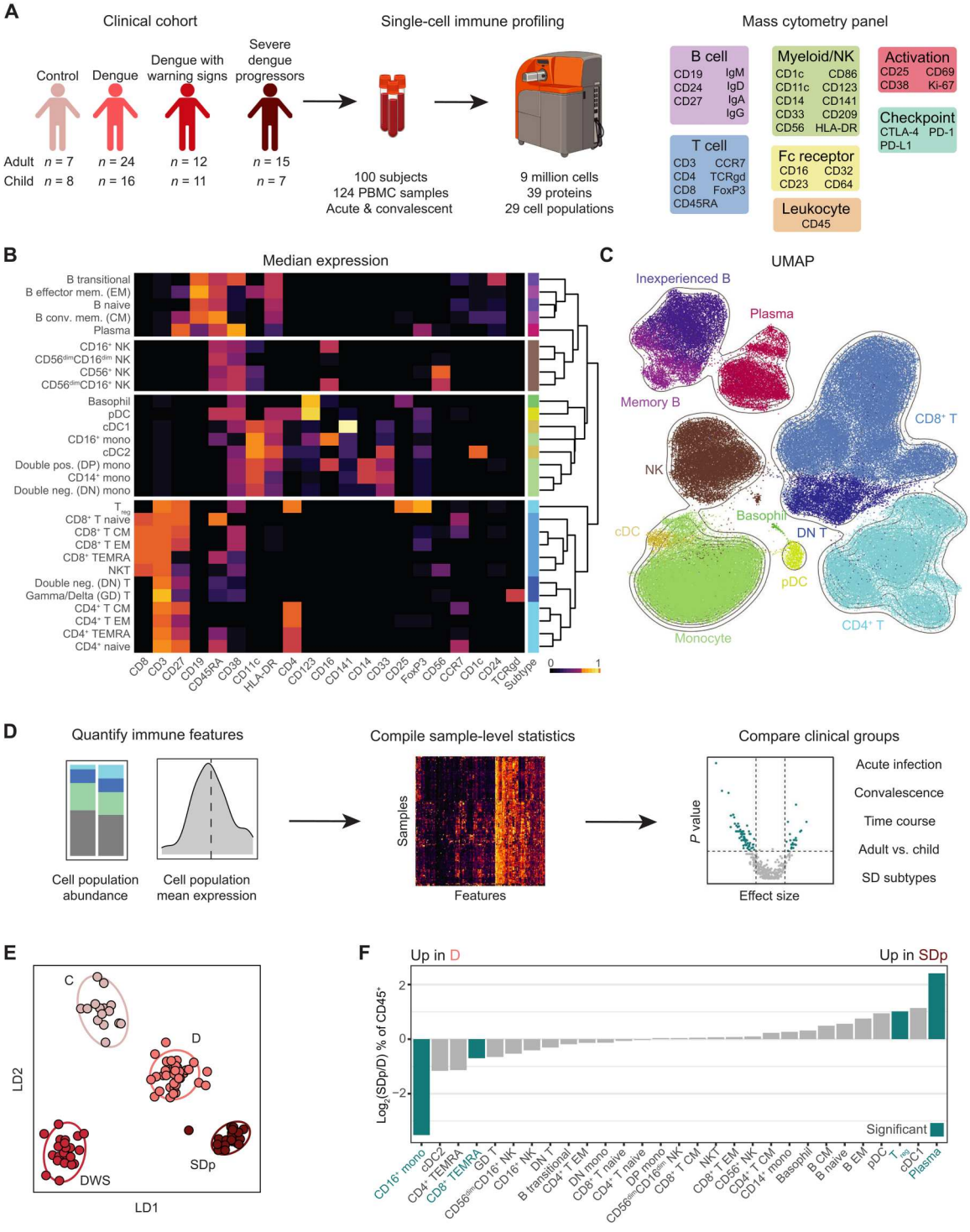

Fig. 1. High-dimensional immune profiling delineates disease severity in dengue infection. (**A**) Experimental approach. Acute and convalescent PBMC samples were collected from a clinical cohort of DENV-infected patients and healthy controls. Samples were analyzed by mass cytometry using an antibody panel targeting proteins expressed by multiple immune cells. (**B**) Heatmap of the median-scaled arcsinh-transformed expression (color coded) of lineage molecules (columns) in cell B, NK, myeloid, and T cell populations (rows) spaced by cell type. Cell subtype color annotation is depicted on the right. PBMCs were equally subsampled by clinical status and patient. (**C**) UMAP generated using all molecules as input colored by cell subtype (B). PBMCs were equally subsampled by clinical status and patient. (**D**) Analysis approach. Immune features were quantified and compiled into summary statistics for each sample. Distribution tests were performed for each feature for various comparisons. (**E**) Linear discriminate analysis separating acute patient samples by clinical status. Dots represent individual patients, and ellipses represent 95% confidence intervals (CIs). The manifold was derived using all features significantly different in pairwise comparisons of clinical statuses. (**F**) Log_2 ratio of median abundances of cell populations (columns) between D and SDp patients of total $CD45^+$ cells. Teal bars indicate significance ($q < 0.05$ and $|effect| > 0.5$) via Wilcoxon rank sum tests. *Q* values represent FDR-corrected *P* values.

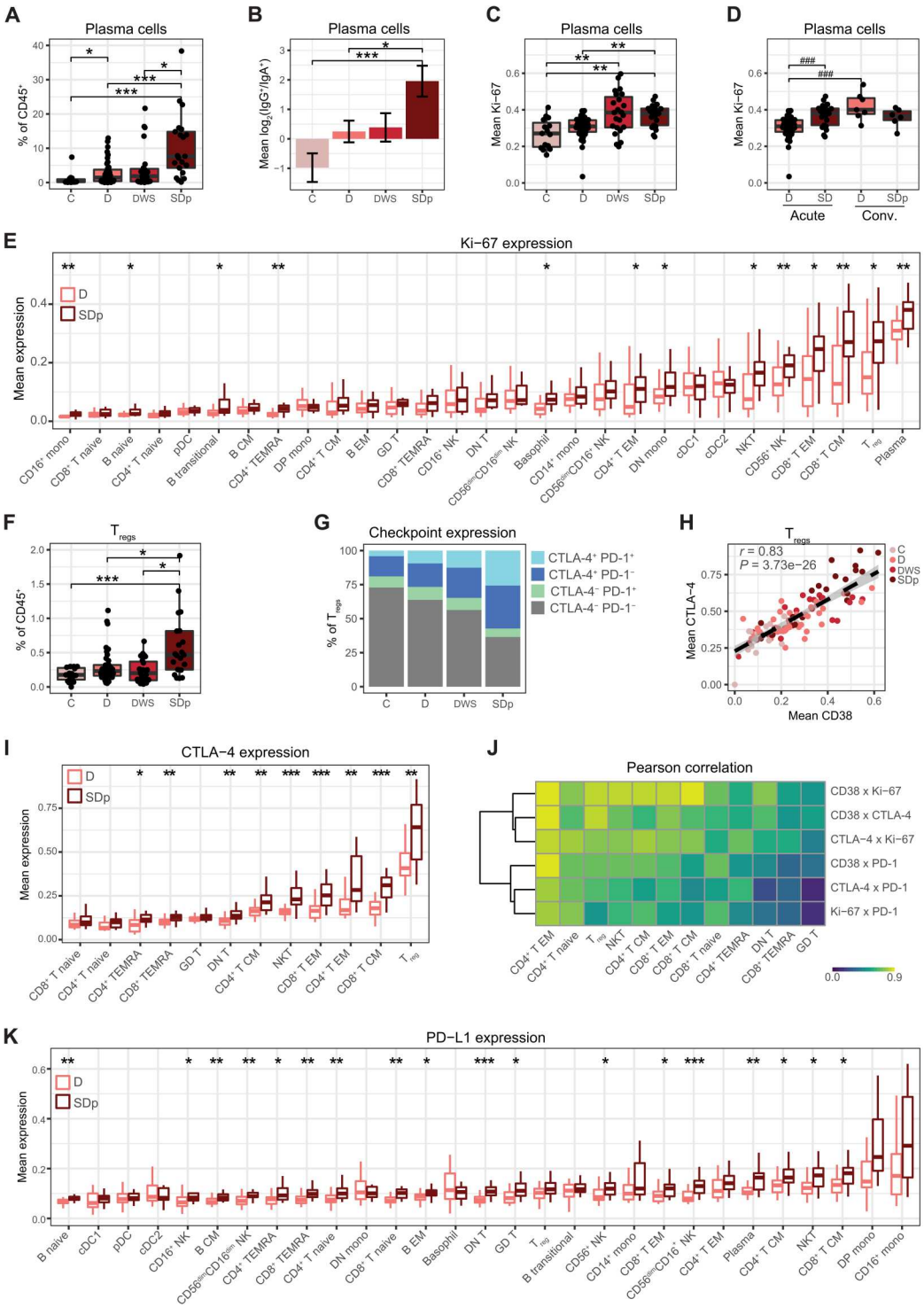

Fig. 2. Immune activation and regulation are simultaneously enriched in acute SDp. (**A** and **F**) Box plots of plasma cell (A) and T_{reg} (F) fraction of $CD45^+$ cells by clinical status. (**B**) Mean $\log_2$ ratio of patient IgG^+ plasma cell abundance to IgA^+ plasma cell abundance by clinical status. Error bars represent SEM. (**C** to **E**, **I**, and **K**) Box plots of mean Ki-67 (C to E), CTLA-4 (I), and PD-L1 (K) expression in acute (C to E, I, and K) and convalescent samples (D) in the indicated cell populations by clinical status. (**G**) Proportion of CTLA-4^+, PD-1^+ T_{regs} by clinical status. Quantifications were derived from an equal subsampling of T_{regs} by clinical status and patient. (**H**) Scatter plot of mean expression of CD38 versus CTLA-4 in T_{regs} by patient (dots), colored by clinical status. Fitting line and CI were derived by linear regression. Pearson correlation coefficient (*r*) and *P* value are shown. (**J**) Pearson correlation coefficients (color) in pairwise analysis of mean expression of checkpoint and activation molecules (rows) by T cell population (columns). All correlations are significant ($q < 0.05$ and $|effect| > 0.5$) except CTLA-4 × PD-1 and Ki-67 × PD-1 in GD T cells. In box plots, center line signifies median, box signifies interquartile range (IQR), and whiskers signify IQR ± 1.5*IQR. Dots in (A), (C), (D), (F), and (H) represent individual patients. $^*q < 0.05$ and $|effect| > 0.5$; $^{**}q < 0.01$ and $|effect| > 0.5$; $^{***}q < 0.005$ and $|effect| > 0.5$; $^{\#\#\#}P < 0.005$ and $|effect| > 1.0$ by Wilcoxon rank sum tests. *Q* values represent FDR-corrected *P* values. C, controls; D, dengue; DWS, dengue with warning signs; SDp, SD progressors.

Since both abundance (Fig. 1F) and Ki-67 expression (Fig. 2E) of T_{regs} were greater in SDp than in D patients, we measured T_{reg} abundance in all disease severity categories. T_{reg} abundance in SDp was greater (median = 0.47%) than in DWS (median = 0.20%, $q = 0.026$), D (median = 0.23%, $q = 0.025$), and C (median = 0.18%, $q = 0.001$) (Fig. 2F), and these differences resolved at convalescence (fig. S2G). The expression of checkpoint molecules (*32*) was also altered in T_{regs}, with higher levels of cytotoxic T lymphocyte–associated protein 4 (CTLA-4) in SDp than in DWS ($q = 0.036$), D ($q = 0.004$), and C subjects ($q = 0.00003$) and PD-1 in SDp than in D ($q = 0.04$) and C subjects ($q = 0.001$) (Fig. 2G). Moreover, CTLA-4 expression was highly correlated with the expression of CD38 ($r = 0.83$, $P = 3.73 \times 10^{-26}$) (Fig. 2H), which was shown to be associated with a highly suppressive T_{reg} phenotype (*33*).

To understand the breadth of checkpoint molecule up-regulation in SDp, we monitored their expression in other T cell populations. CTLA-4 was more highly expressed in SDp over D in 9 of 12 T cell subtypes ($q < 0.05$) (Fig. 2I). PD-1 expression demonstrated similar trends, although it was significantly increased in SDp over D in only 2 of the 12 T cell populations ($q < 0.05$) (fig. S2H). As in the T_{regs}, we observed a significant correlation ($q < 0.05$) between the expression of activation proteins, CD38 and Ki-67, and checkpoint proteins, CTLA-4 and PD-1, in all T cell populations (Fig. 2J). Moreover, the checkpoint ligand PD-L1 was more highly expressed in SDp relative to D in 18 of 29 cell populations ($q < 0.05$), spanning B, T, and NK cell populations, but not myeloid cells (Fig. 2K). Increased CTLA-4 expression in SDp resolved in all T cell populations at convalescence (fig. S2I), whereas increased PD-L1 expression persisted in some T and NK cell populations (fig. S2J). These findings reveal substantial and simultaneous immune activation and regulation uniquely occurring in SDp.

Diminished HLA-DR and increased CD64 expression on myeloid cells are hallmarks of SD progression

Next, we further probed alterations in myeloid cell abundance and function. Within the monocyte population, the fraction of $CD16^+$ monocytes was lower in SDp than in D ($q = 0.0003$) and C ($q = 0.0008$) (table S2) with trends toward a reduced double-negative (DN; $CD14^-CD16^-$) monocyte fraction and expanded $CD14^+$ monocyte fraction, which will need to be explored in larger cohorts (Fig. 3A). Beyond differences in cell subset abundance, myeloid cells from D and SDp patients exhibited differential expression of several functional markers (Fig. 3B). Ki-67 in $CD16^+$ and DN monocytes, CD38 in these two monocyte subtypes and cDC2s, and the Fcγ receptor (FcγR) CD64 in cDC2s and DN monocytes were higher in SDp than in D ($q < 0.05$). CD141 (thrombomodulin), an anti-inflammatory factor (*34*), was increased in $CD14^+$ monocytes in SDp over D ($q = 0.008$). A trend, albeit statistically nonsignificant, for greater PD-L1 expression on several myeloid cell subtypes was also detected (Fig. 3B). In contrast, CD209 [DC-SIGN, a DENV attachment factor (*35*)] was lower on cDC2s in SDp relative to D patients ($q = 0.015$). More prominent, however, was the reduction in human leukocyte antigen (HLA)–DR expression in SDp relative to D patients in all myeloid cell subtypes, reaching statistical significance in DN monocytes, $CD16^+$ monocytes, and cDC2s ($q < 0.05$; Fig. 3, B and C). In contrast to myeloid cells, several NK cell subtypes expressed higher levels of HLA-DR in SDp relative to D patients ($q < 0.05$; Fig. 3C), suggesting increased functional activity in SDp, as previously shown in other infectious disease models (*36*, *37*). While the differences in proportional myeloid cell subtype abundance and HLA-DR expression largely resolved at convalescence, increased expression of CD64 in SDp over D persisted in several myeloid subsets ($P < 0.05$; fig. S3, A to C and E).

Given the changes in expression, we then asked whether the proportional abundance of cDC2s out of cDCs also differed by severity. We found lower abundance in SDp than in DWS ($q = 0.026$), D ($q = 0.008$), and C ($q = 0.002$) (Fig. 3D), with resolution at convalescence (fig. S3D). The strongest pairwise correlation of cDC2 features appeared between CD64 expression and detected IgG ($r = 0.83$, $P = 3.73 \times 10^{-26}$; Fig. 3E). Subsampling cDC2s from distinct disease categories revealed that at the single-cell level, CD64 and IgG were more strongly correlated in DENV-infected patients than control cells during acute infection (Fig. 3G), whereas no such correlation was detected in convalescent samples (fig. S3F). Since DCs do not produce antibodies, this finding may reflect serum antibodies bound by cell surface receptors (*38*), suggesting that CD64 expression may in part mediate the observed binding of IgG by myeloid cells. The detected level of other antibody isotypes was not correlated with CD64 expression (fig. S3G), in agreement with the known function of CD64 as an IgG-specific FcγR (*39*). Similar correlations between CD64 expression and IgG detection were observed on monocytes in acute samples (Fig. 3, F and H) and resolved at convalescence (fig. S3H).

Together, these findings reveal that SD progression is associated with alterations in the proportional abundance of myeloid cell populations and diminished expression of HLA-DR concurrent with increased expression of the FcγR CD64 in correlation with increased IgG antibody levels on myeloid cells, possibly mediating ADE of infection (*40*). Our attempts to test the latter hypothesis by measuring viral abundance in myeloid and other candidate DENV target cells (*10*, *41*) were, however, unsuccessful (see Supplementary Text). Moreover, while DENV viral load measured in patient serum via reverse transcription quantitative polymerase chain reaction (RT-qPCR) was comparable between distinct disease categories in our cohort (fig. S4A and table S1.1), this finding has to be interpreted cautiously since we did not monitor viremia over time and the number of samples was relatively small.

Differences in the innate immune response to DENV infection between D and SD are exaggerated in children

While some studies have shown higher fatality rates in SDp children than adults (*42*), others have reported a greater mortality in adult patients in association with various comorbidities (*23*). To explore differences in immune responses between D and SDp adults and children (under 17 years), we compared cell population abundances and functional marker expression by distribution tests (table S4). The abundance of cytotoxic $CD56^{dim}CD16^+$ NK cells was significantly lower in SDp relative to D children ($P = 0.002$) but not adults ($P = 0.42$; Fig. 4, A and B). Moreover, the expression of the FcγR, CD16, was lower on $CD56^{dim}CD16^+$ NK cells in SDp children ($P = 0.002$), but not adults ($P = 0.16$), consistent with receptor shedding indicative of cell activation (Fig. 4C) (*43*, *44*). The drop in $CD56^{dim}CD16^+$ NK cells in SDp children was accompanied by a proportional expansion of $CD56^+$ NK cells out of total NK cells ($P = 0.014$; Fig. 4D and table S4), suggesting that NK cells may be skewed toward a less cytotoxic, more inflammatory phenotype (*36*). The fraction of $CD56^{dim}CD16^+$ NK cells out of total NK cells was almost sufficient to stratify the cohort by disease severity in children, but not adults (Fig. 4D and fig. S5A). HLA-DR was more highly expressed on $CD56^{dim}CD16^+$ NK cells in SDp children but not adults, further supporting increased functional activity of these cells (Fig. 4E) (*36*, *37*).

The abundance of $CD16^+$ monocytes was lower in SDp than in D patients in both adults and children (Fig. 4A and fig. S5B). Nevertheless, HLA-DR was lower on $CD16^+$ and DN monocytes in children only (Fig. 4E), despite the smaller sample size, suggesting a greater impairment in antigen presentation in SDp children than in SDp adults.

Plasma cell abundance appeared higher in SDp than in D in both adults and children, but the difference was statistically significant in adults only (Fig. 4, A and F). While this difference could, in theory, be explained by the smaller number of pediatric samples analyzed,

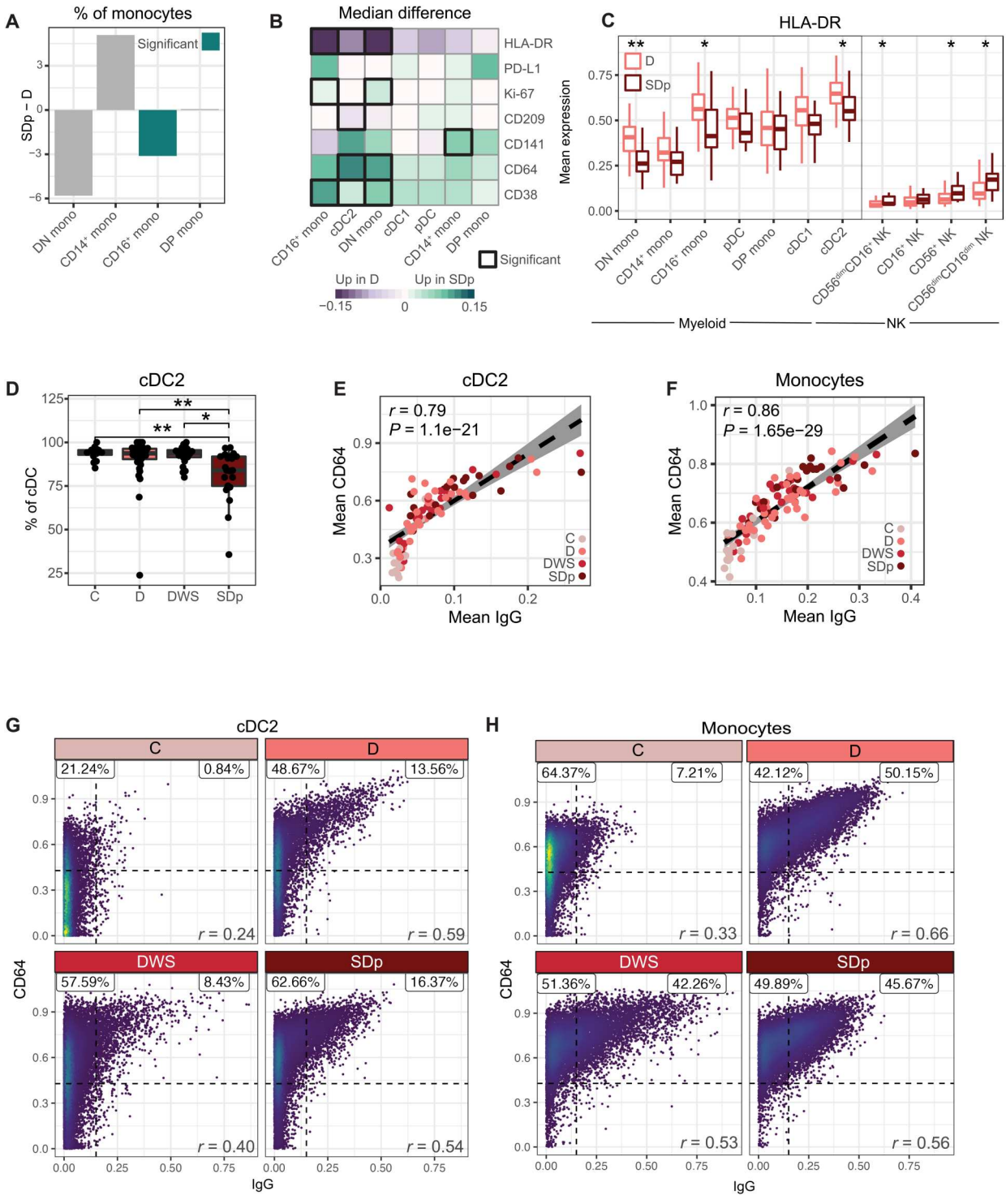

Fig. 3. Diminished HLA-DR and increased CD64 expression on myeloid cells are hallmarks of SDp. (**A**) Difference in median relative abundances of monocyte subtypes (columns) between SDp and D patients of total monocytes. (**B**) Difference in cohort median of patient mean expression between SDp and D across molecules (rows) in myeloid cell populations (columns). Black boxes depict significance ($q < 0.05$ and |effect| > 0.05). (**C**) Box plots of mean HLA-DR expression in the indicated myeloid and NK cell subtypes by clinical status. (**D**) Box plots of cDC2 fraction of cDCs by clinical status. Dots represent individual patients. (**E** to **H**) Scatter plots of mean (E and F) or single-cell CD64 expression versus IgG detection in acute infection on cDC2s (E and G) and monocytes (F and H) by either patient (dots, colored by clinical status) (E and F) or clinical status (G and H). Fitting line and CI in (E) were derived by linear regression. Percent proportion of cells in each quadrant, derived from an equal subsampling of cells by clinical status and patient, are shown in (F) and (G). In box plots, center line signifies median, box signifies IQR, and whiskers signify IQR ± 1.5*IQR. Teal bars (in A) and asterisks (in C and D) indicate significance: *$q < 0.05$ and |effect| > 0.5; **$q < 0.01$ and |effect| > 0.5 by Wilcoxon rank sum tests. *r* and *P* values (E to G) were calculated by Pearson correlation.

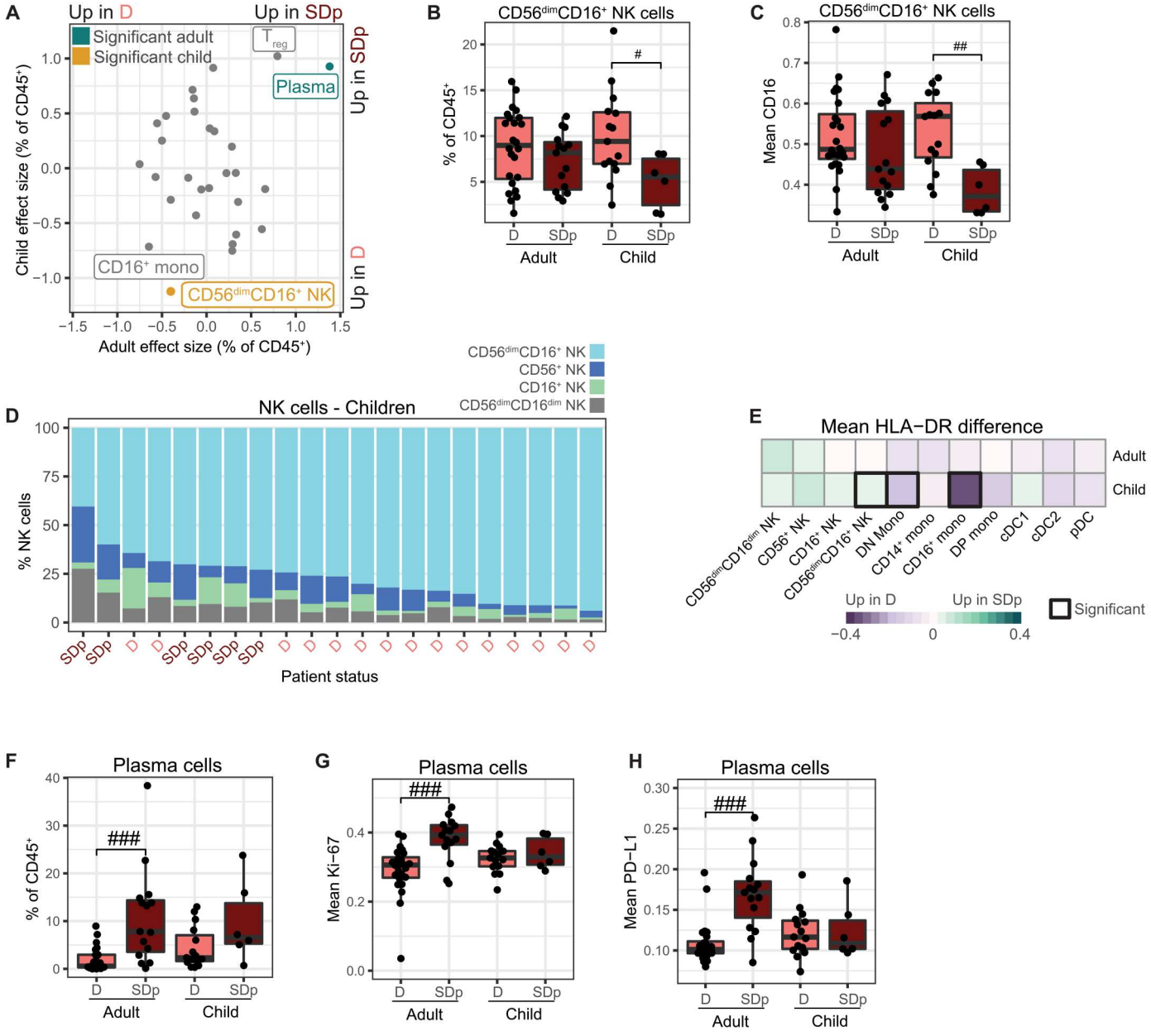

Fig. 4. Differences in the innate immune response to DENV infection in D and SDp are exaggerated in children. (**A**) Effect size in comparison of cell population abundances (dots) in SDp and D in adults (*x* axis) and children (*y* axis). Teal and gold indicate significance in adults and children, respectively. ($P < 0.05$ and |effect| > 1.0). (**B** and **F**) Box plots of CD56^{dim}CD16^{+} NK cell (B) and plasma cell (F) fractions of CD45^{+} cells by clinical status and age. Dots represent individual patients. (**C**, **G**, and **H**) Box plots of mean CD16 (C), Ki-67 (G), and PD-L1 (H) expression in the indicated cells by clinical status and age. Dots represent patients. (**D**) Proportion of NK cell subtypes in children ordered by CD56^{dim}CD16^{+} NK cell abundance. Columns represent individual patients, labeled by clinical status. (**E**) Difference in cohort mean of patient mean HLA-DR expression between SDp and D across cell populations (columns) by age (rows). Black boxes indicate significance ($P < 0.05$ and |effect| > 1.0). In box plots, center line signifies median, box signifies IQR, and whiskers signify IQR ± 1.5*IQR. $^{\#}P < 0.05$ and |effect| > 1.0; $^{\#\#}P < 0.01$ and |effect| > 1.0; $^{\#\#\#}P < 0.005$ and |effect| > 1.0 by Wilcoxon rank sum tests.

the effect size was greater in adults (1.38) than in children (0.93). Moreover, the expression levels of Ki-67 and PD-L1 in plasma cells were higher in SDp adults relative to D adults, but comparable in SDp and D children (Fig. 4, A, G, and H), suggesting that the observed differences in plasma cell responses between adults and children may be biologically relevant.

While CD8^{+} TEMRA abundance was reduced in SDp in the combined cohort (Fig. 1F), this difference did not reach statistical significance in the distinct age groups (Fig. 4A and fig. S5C). Nevertheless, HLA-DR and CD38 were more highly expressed in CD8^{+} TEMRAs in SDp children ($P < 0.05$), but not adults (fig. S5, D and E), signifying greater cell activation. In contrast, neither abundance of (Fig. 4A and fig. S5, B and F) nor expression markers (table S4) on

$CD16^+$ monocytes and T_{regs} were significantly altered between SDp adults and children.

These findings reveal both overlapping and distinct immune responses between SDp adults and children and point to increased plasma cell abundance and proliferation in SDp adults, yet more inadequate expansion of activated cytotoxic NK cells, and more prominent $CD8^+$ TEMRA activation and reduced antigen presentation on myeloid cells in SDp children.

Immune cell composition stratifies patients by SD categories

The 2009 WHO definition of SD includes the presence of severe bleeding or plasma leakage, somewhat similar to the prior definitions of DHF and DSS, respectively, but also OI involving the liver, brain, and heart (WHO, 2012). To compare the host response to DENV between these SD categories, we measured cell type abundance and protein expression in patients who once progressed to SD manifested with hemorrhages and/or vascular leak (DHF/DSS, $n = 15$) and those with organ (liver) impairment (OI, $n = 4$) (fig. S6 and table S5). Children and adults were similarly represented in these two groups (fig. S6). Two patients who presented with both DHF and OI were not included in this analysis. The abundance of immune cell populations was markedly altered between DHF/DSS and OI patients, with higher abundances of cDC1s, cDC2s, and T_{regs} in OI yet higher abundance of plasma cells in DHF/DSS ($P < 0.05$; Fig. 5A).

The abundances of cDC1s and cDC2s in OI resembled and were not statistically different from C ($P = 0.36$ and $P = 0.18$). cDC1 and cDC2 abundances were, however, lower in DHF/DSS relative to C ($P = 0.0001$ and $P = 0.000001$) and comparable to the levels of D and DWS patients (Fig. 5B). Ordering patients by total cDC abundance nearly perfectly stratified the two SD categories (Fig. 5C). In addition, cDC1s from OI samples expressed a higher Ki-67 level ($P = 0.01$) but lower CD64 level ($P = 0.02$; Fig. 5D), suggesting that while expanded and more proliferative relative to DHF/DSS, they may have decreased antibody binding capacity.

Beyond myeloid cells, plasma cell abundance was greater in DHF/DSS than in OI (and C, D, and DWS) patients ($P < 0.05$; Fig. 5E). The Ig isotype usage in plasma cells was also different, with predominately IgG enrichment in DHF/DSS patients versus an increase in IgM enrichment in OI ($P = 0.04$), revealing a less class-switched, more naïve humoral response in OI (Fig. 5F). In contrast, T_{regs} were more abundant in OI than in DHF/DSS, DWS, D, and C samples ($P < 0.05$; Fig. 5G), yet there was no significant difference in CTLA-4 and PD-1 expression between the two SD categories (table S5). OI is thus skewed toward T_{regs}, whereas DHF/DSS is skewed toward plasma cells. Plotting these two features on a biaxial plot nearly perfectly stratified the two SD categories (Fig. 5H). Although the numbers are small, these differences in immune cell composition and activation support that DHF/DSS and OI may represent distinct syndromes associated with differential immunopathogenesis.

The temporal switch of innate and adaptive immune activation and concurrent immune regulation are dysregulated in acute SDp

To capture the temporal dynamics in the host response during acute infection, we monitored the kinetics of immune activation and regulation in SDp and D on days 3 to 8 after fever onset (fig. S7, A and B). For each individual day, we used samples from a 3-day rolling window (tables S1.4 and S6) to account for error in the timing of patients' self-reported symptom onset. We performed Wilcoxon rank sum tests and calculated effect size between SDp and D for each rolling day window for all features (table S6).

Given the substantial increase in immune activation seen in SDp over D (Fig. 2E and fig. S2D), we asked whether this difference varied throughout the course of infection. We assessed the difference in mean expression of the activation marker, CD38, by time and cell population and found significant differences in T and myeloid cell populations ($P < 0.05$; Fig. 6A). Three clusters emerged when the data were hierarchically clustered by cell population: populations with higher CD38 expression in SDp early in acute infection, populations with higher CD38 in SDp late in acute infection, and populations with similar levels of CD38 at all time points. The first cluster consisted primarily of memory T cell populations, whereas the second cluster was composed primarily of myeloid populations.

To better understand these dynamics, we plotted the mean expression of CD38 in D and SDp over time in a representative cell population from each of the first two clusters: $CD8^+$ T EM (higher early in SDp) and $CD14^+$ monocytes (higher late in SDp) (Fig. 6B). In $CD8^+$ T EM cells, while CD38 was continuously more highly expressed starting on day 3 in SDp, its expression in D patients was low early on but gradually increased to a similar level as SDp by day 8, with the difference peaking on day 4 after fever onset. This early $CD8^+$ T EM cell activation could be explained in part by the higher percentage of secondary infections among SDp (fig. S1A). In contrast, in $CD14^+$ monocytes, CD38 mean expression was initially high in both D and SDp, yet while it steadily declined over the course of acute infection in D, in SDp, it remained high throughout the acute infection, with the difference peaking on day 7. CD64 expression on myeloid cells followed similar trends to CD38, with significantly higher expression in SDp in cDC2s and DN monocytes at late acute time points ($P < 0.05$; fig. S7C). These shifts in the kinetics of the adaptive and innate immune responses were not limited to T and myeloid cells, but also appeared in plasma cell abundance and isotype usage, as well as the expression of the stimulatory receptor, CD69 (*45*), on NK cells (Fig. 6C).

Next, we monitored the kinetics of immune regulation during the course of acute DENV infection. PD-L1 expression on NK cells was comparable in D and SDp patients on day 3, yet in D patients, it steadily declined through day 8, whereas in SDp, its expression peaked on day 5, an intermediate time point between the first and second clusters, before diminishing (Fig. 6C). This pattern was conserved in nearly every immune cell population (Fig. 6D), although the magnitude of PD-L1 expression varied (fig. S7D). This temporal pattern of PD-L1 expression was perturbed only in transitional B cells, which peaked at day 7 in D, rather than early in infection. This antigen-inexperienced population has been shown to be enriched for immunoregulatory cytokine production (*46*), which may coincide with their unique checkpoint expression profile. The CTLA-4 expression pattern was more similar to that of CD38 (Fig. 6, A and E), with higher expression in T_{regs}, $CD4^+$ T EM, $CD8^+$ T EM, and $CD8^+$ T CM in SDp primarily at earlier time points ($P < 0.05$) (Fig. 6E). This temporal coordination between CTLA-4 and CD38 in T cells was consistent with a high degree of correlation measured between these two markers (Fig. 2, H and J). CTLA-4 and PD-1 expression levels in T_{regs} were higher in SDp at

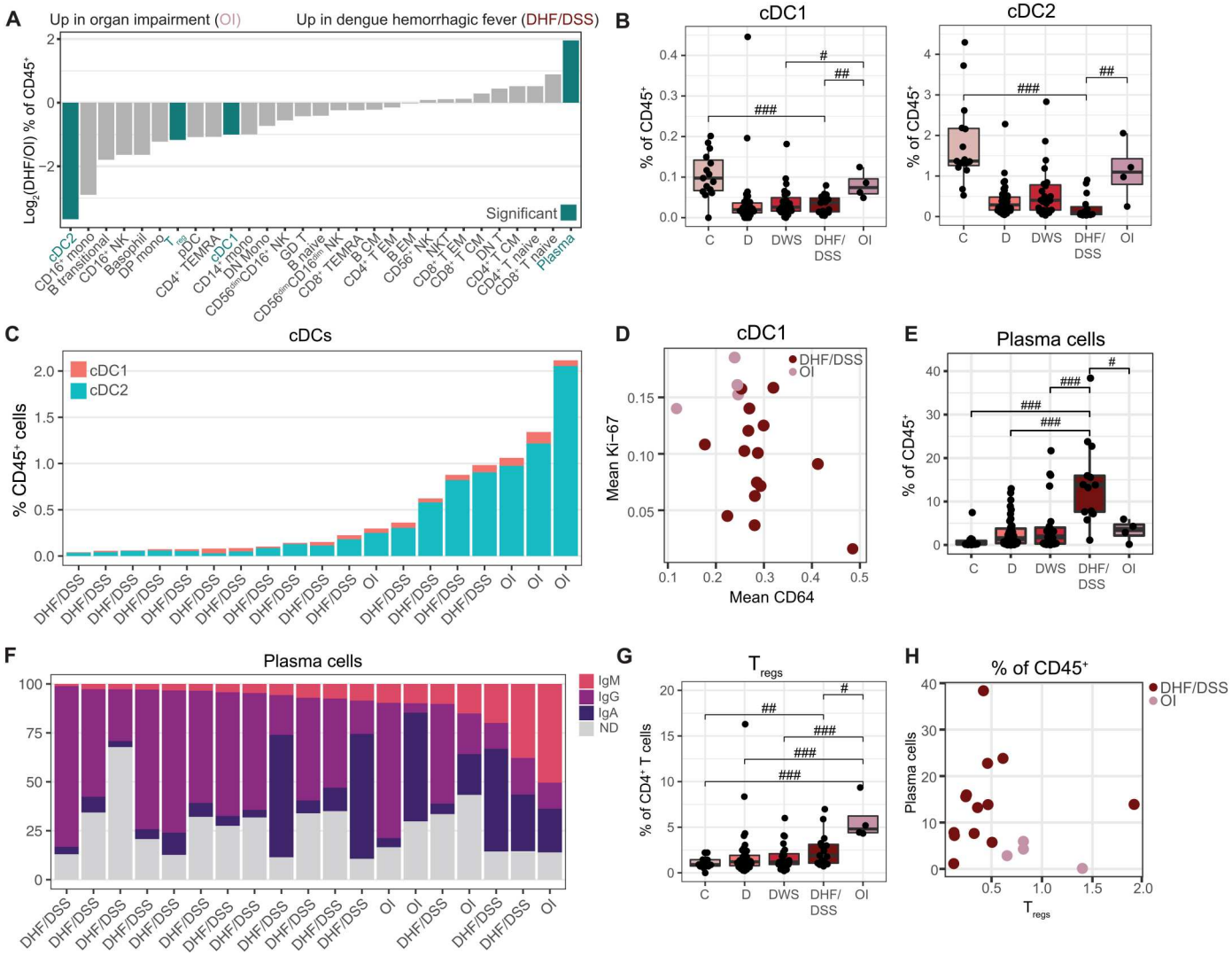

Fig. 5. Immune cell composition stratifies patients by SD categories. (**A**) Log_2 ratio of median abundances of cell populations (columns) between patients with DHF/DSS and OI. Teal bars indicate significance ($P < 0.05$ and |effect| > 1.0). (**B**, **E**, and **G**) Box plots of cDC1 (B, left), cDC2 (B, right), plasma cell (E), and T_{reg} (G) fractions of $CD45^+$ cells by clinical status. Dots represent individual patients. (**C**) Proportion of cDC populations ordered by total abundance. Columns represent individual patients, labeled by SD syndrome. (**D**) Mean CD64 and Ki-67 expression in cDC1s by patient (dots), colored by SD syndrome. (**F**) Proportion of isotype usage in plasma cells ordered by IgM usage. Columns represent individual patients labeled by SD syndrome. ND, isotype not determined because of low expression. (**H**) Scatter plot of plasma cell and T_{reg} abundance by patient (dots), colored by SD syndrome. In box plots, center line signifies median, box signifies IQR, and whiskers signify IQR ± 1.5*IQR. $^{\#}P < 0.05$ and |effect| > 1.0; $^{\#\#}P < 0.01$ and |effect| > 1.0; $^{\#\#\#}P < 0.005$ and |effect| > 1.0 by Wilcoxon rank sum tests. OI, organ impairment; DHF/DSS, dengue hemorrhagic fever/dengue shock syndrome.

early time points ($P < 0.05$) before gradually decreasing, whereas in D patients, both proteins were expressed at relatively lower levels throughout infection (Fig. 6F). Likewise, the overall T_{reg} abundance peaked early in SDp ($P < 0.05$), while it remained stably lower in D.

HLA-DR showed no obvious temporal patterns, yet it was significantly lower in multiple myeloid cell populations in SDp relative to D patients throughout the disease course ($P < 0.05$; fig. S7E). Moreover, the proportional abundance of $CD16^+$ and DN monocytes, on which HLA-DR expression was lower in SDp, was low in SDp throughout the infection, whereas in D patients, it started high and gradually decreased (fig. S7F). The abundance of $CD56^{dim}CD16^+$ NK cells was also lower in SDp than in D during acute infection (fig. S7G).

On the basis of these findings, we propose a hypothetical model in which D is characterized by early activation of the innate immune response predominated by expansion of $CD16^+$ monocytes, which, along with other myeloid cells, present antigen adequately via HLA-DR expression, as well as increased DENV target cell killing via cytotoxic NK cells. This response then wanes as the adaptive immune system becomes increasingly stimulated, with minimal activation of regulatory signals. In contrast, in SDp, there is rapid expansion of IgG-producing plasma cells (more pronounced in adults) and memory T cell activation (more pronounced in children). Moreover, a more activated T_{reg} population emerges concurrently with inadequate expansion of $CD16^+$ monocytes and reduced antigen presentation capacity in myeloid cells (particularly in children) as

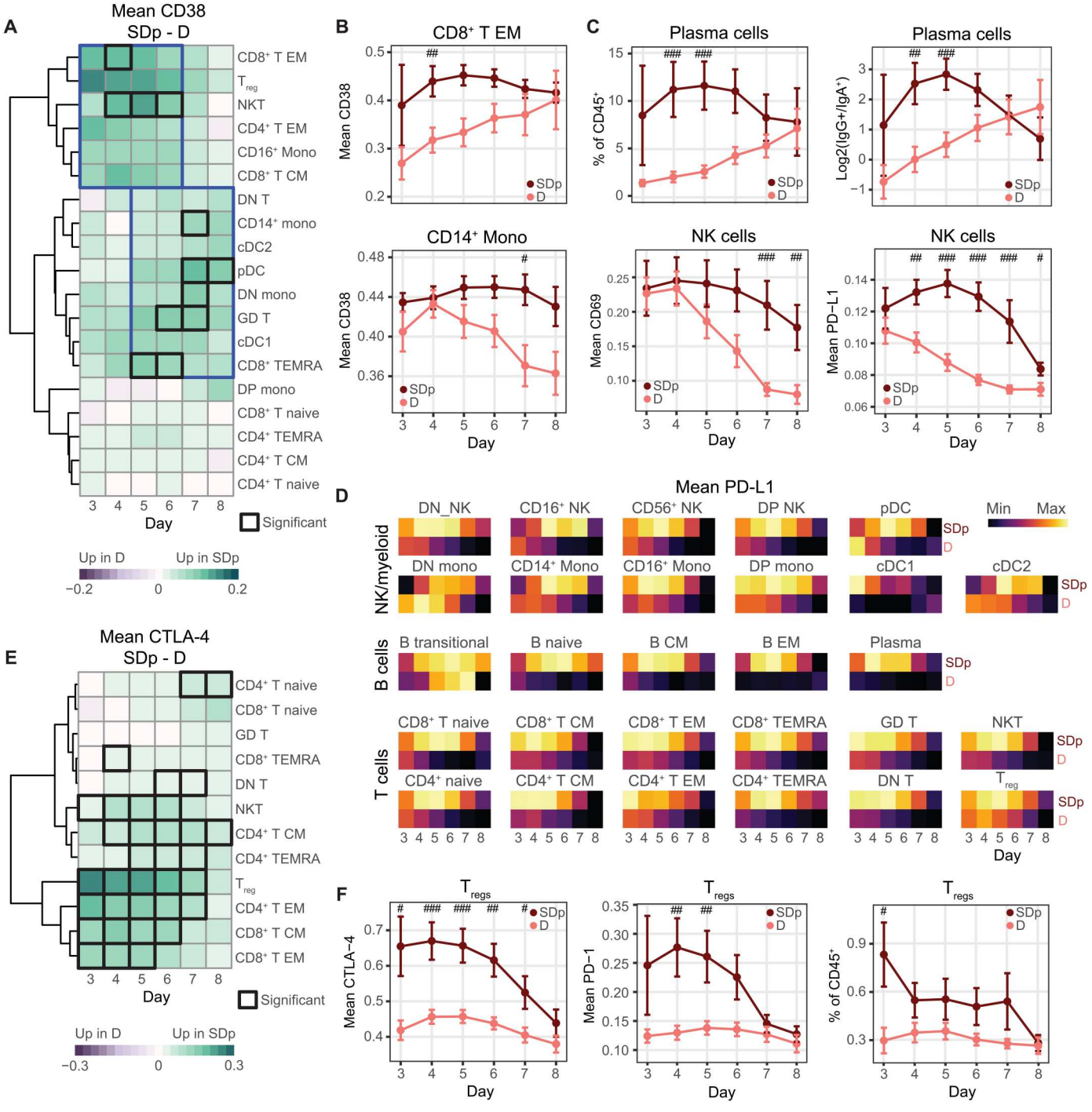

Fig. 6. The temporal switch of innate and adaptive immune activation and concurrent immune regulation is dysregulated in SDp. (**A** and **E**) Difference in cohort mean of patient mean CD38 (A) and CTLA-4 (E) expression between SDp and D across cell populations (rows) by day (columns). Black boxes depict significance ($P < 0.05$ and |effect| > 1.0). Blue boxes group time points and populations with similar trends. (**B**) Cohort mean of patient mean CD38 expression in $CD8^+$ T EM (top) and $CD14^+$ monocytes (bottom) by clinical status and day. (**C**) Cohort mean of plasma cell abundance (top center), $\log_2$ ratio of IgG^+ to IgA^+ plasma cell abundance (top right), and mean CD69 (bottom left) and PD-L1 (bottom right) expression in NK cells by clinical status (color) and day (columns). (**D**) Cohort mean of patient mean PD-L1 expression (color) by day (columns) and clinical status (rows), separated by cell population (tiles). Each tile is individually scaled. (**F**) Cohort mean of patient mean CTLA-4 (left) and PD-1 (center) expression in T_{regs} and abundance of T_{regs} (right) by clinical status and day. $^{\#}P < 0.05$ and |effect| > 1.0; $^{\#\#}P < 0.01$ and |effect| > 1.0; $^{\#\#\#}P < 0.005$ and |effect| > 1.0 by Wilcoxon rank sum tests. Error bars represent SEM.

well as skewing of NK cell responses from cytotoxic to proinflammatory (particularly in children). Together, this uncoordinated immune response is ineffective in controlling viral spread and at the same time increases proinflammatory signals causing tissue injury and leading to worse prognosis (Fig. 7). Since based solely on expression patterns, this model requires further functional validation.

DISCUSSION

The pathogenesis of SD remains poorly understood. Here, we comprehensively characterized the human immune response to DENV infection at single-cell resolution. Leveraging the clinical diversity of the Colombia dengue cohort to capture real-world heterogeneity revealed unique and overlapping responses between various disease categories and age groups during the course of natural infection.

Previous studies using similar approaches to monitor natural DENV infection have uncovered increased type I IFN responses (*47*), up-regulation of activation markers including CD38 and CD169 on myeloid cells (*48*), and temporal shifts in B and T cell phenotypes (*49*). However, these studies either did not include SD patients, combined SD with D patients in comparison with controls, or studied focused elements of the immune response. Several features of our cohort and workflow have provided a unique opportunity to probe SD pathogenesis. First, our study included 22 SD patients, 19 of whom were enrolled before progression to SD and 3 after progression to SD yet within 5 days of symptom onset, enabling monitoring of the host response early in the course of SD. Second, enrolling adults and children enabled identification of age-dependent and independent determinants in the host response to DENV. Third, comparing SDp manifesting with OI to those with DHF/DSS has shone light on this previously unstudied aspect, defining these conditions as likely immunologically distinct syndromes. Moreover, comparing D and SDp to DWS patients, a population that has been understudied to date, revealed that the phenotypes of DWS patients largely overlap with those of D rather than SDp. Beyond clinical heterogeneity, we captured immune heterogeneity using an antibody panel that enabled clustering of a diverse array of cell subtypes. Last, applying this analysis to longitudinal patient samples collected during the disease course and at convalescence facilitated a comprehensive profiling of both the magnitude and kinetics of the immune responses to DENV infection.

Our findings revealed greater and more rapid activation of a memory response in SDp than D patients. A prominent expansion of proliferating IgG-secreting plasma cells, as previously described (*14*, *50*), was measured early in the course of SDp, whereas the magnitude of this response was lower and its kinetics was slower in D

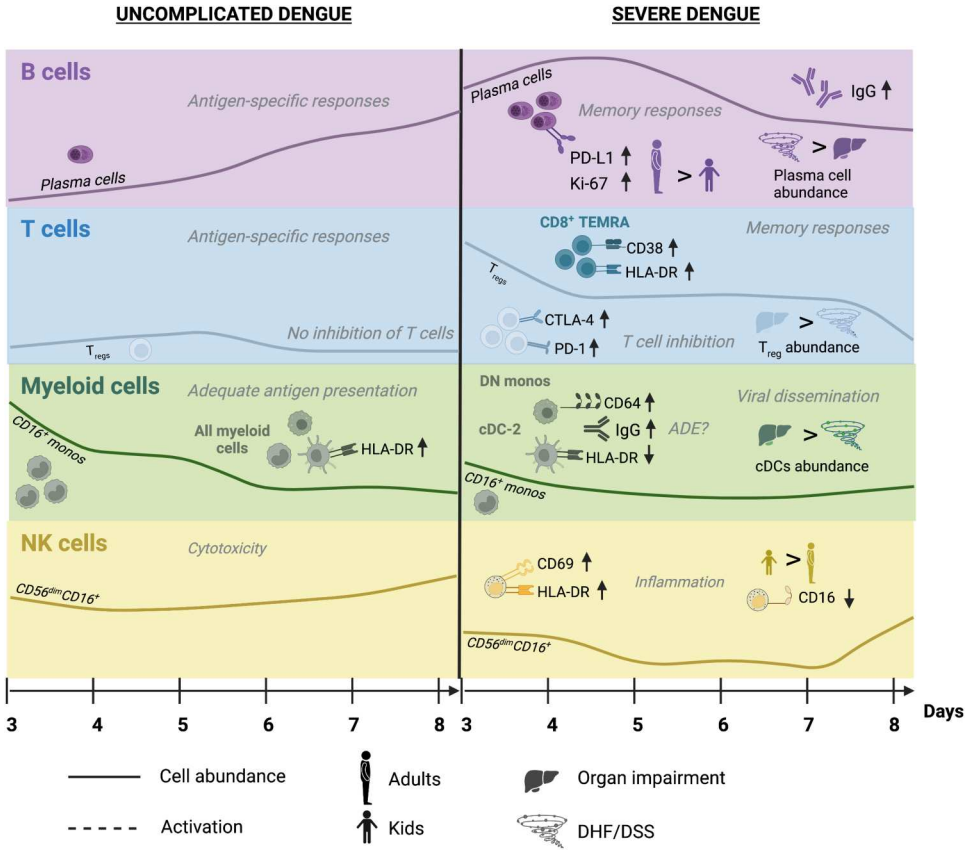

Fig. 7. Proposed hypothetical model for differential immune responses between uncomplicated and SD patients. Schematic of the kinetics and magnitude of cell subtype abundance and protein marker expression during acute D and SD infections. Most prominent differences in innate and adaptive immune responses are shown. Prominent differences in immune responses between adults and children and SDp with DHF/DSS and OI are also depicted. Black titles depict findings detected in the current study; gray titles depict predicted phenotypes that require further functional validation.

patients. Similarly, SDp, particularly children, demonstrated increased CD38 and HLA-DR expression on $CD8^+$ T EM and/or TEMRA cells, suggesting more robust activation of mature T cell responses. These findings support the original antigenic sin theory in which preexisting memory B and T cells generated from a prior heterotypic DENV infection skew the early immune response upon secondary infection toward a less specific yet more proinflammatory phenotype leading to disease progression (*51*).

Monocyte subsets from SDp expressed higher levels of CD38, whose binding to CD31 on platelets and endothelial cells has been shown to facilitate adhesion and migration across the endothelial barrier (*33*), suggesting a possible role in promoting inflammation and/or vascular leakage. Concurrent with increased inflammatory signals, our findings provide evidence for impaired antigen presentation by myeloid cells in SDp. While $CD16^+$ monocyte abundance in D was maintained at similar levels to controls, in SDp, despite increased Ki-67 expression, their abundance was lower than in D. This inadequate expansion of cells with antiviral functions suggests potential impairments in scavenging infected cells, neutrophil recruitment, and patrolling, leading to reduced viral clearance and antigen presentation in SDp (*52*, *53*). Notably, nonclassical monocytes demonstrated reduced abundance in SDp and distinct transcriptomic signatures in DENV-infected individuals in an Indian dengue cohort, highlighting the generalizability of these findings across diverse genetic backgrounds (*54*). The lower expression of HLA-DR on $CD16^+$ (and DN monocytes and cDC2s) in SDp provides additional evidence for impaired antigen presentation by these myeloid cell subtypes.

Since CD16 (type III FcγR) facilitates phagocytosis and is implicated in ADE of DENV infection (*40*), the drop in $CD16^+$ monocyte abundance may also reflect infection-induced cell death. The reduced proportional abundance of cDC2s (out of cDCs) in SDp suggests possible target cell killing or apoptosis and DENV enhancement in cDC2s. CD64 (high-affinity type I FcγR) was more highly expressed in SDp, particularly on cDC2s, and its expression level was highly correlated with detected IgG on these cells, suggesting a role in ADE. This finding appeared specific to CD64, as the expression of CD32, another activating FcγR implicated in ADE (*30*, *55*, *56*), was comparable across severity categories. It is also tempting to speculate that the lower expression of the DENV co-receptor CD209 on cDC2s resulted from virus-receptor complex internalization. These findings agree with prior knowledge that cDC2s, but not cDC1s, are permissive to infection with other enveloped, endocytic viruses (*57*). Our findings propose candidate specific cell types and receptors that drive ADE of infection. Nevertheless, since our attempts to detect viral proteins via mass cytometry were unsuccessful, we were unable to identify DENV target cells and explore functional differences between infected and bystander cells. It is likely that high viral titers combined with viral components shed into plasma made the detection of genuinely infected dengue cells indistinguishable from the background milieu (fig. S4D).

Our findings reveal a marked expansion of T_{regs} displaying significantly higher levels of the effector molecules CTLA-4, PD-1, and CD38 in SDp versus D. Somewhat surprising at an early disease stage, this T_{reg} expansion may be driven in part by the rapid activation of myeloid and plasma cells. The higher expression of CD141, an anti-inflammatory factor typically expressed on cDC1s, on $CD14^+$ monocytes in SDp may enhance this T_{reg} response. CD141 expression on circulating monocytes was shown to induce T_{reg} responses in other disease models (*58*, *59*). HLA-DR^{low} $CD14^+$ monocytes, a regulatory myeloid cell subtype that trended toward expansion in SDp, may also promote T_{reg} expansion, as shown in other viral infections (*60*, *61*).

T_{regs} were previously reported to expand in D patients relative to healthy controls (*62*, *63*), yet their role in disease progression remained unclear. Whereas a previous study demonstrated a protective effect via inhibition of vasoactive cytokines (*62*), another showed no correlation between disease severity and a less suppressive T_{reg} phenotype (*63*). Our findings suggest a more suppressive phenotype associated with SD (*33*). We observed similar findings in other T cell populations, indicating a globally inhibited T cell response, which may be associated with SD progression. The lower expression of HLA-DR on myeloid subtypes in SDp provides additional evidence for the association of SD with suppressed T cell stimulation via impaired antigen presentation.

On one hand, a suppressive T_{reg} response could be detrimental early in the disease course by inhibiting protective antiviral responses via apoptosis of antigen-specific T cells concurrent with inhibition of T_{reg} cell death (*64*, *65*), thereby extending uncontrolled viral replication and enhancing pathology. Increased expression of CTLA-4 and PD-L1 on T cells has been associated with Ebola virus disease fatality (*66*), and polymorphisms in the CTLA-4 gene are associated with SD progression (*67*). On the other hand, suppression of proinflammatory signals may protect from cytokine storm and/or tissue injury. T_{reg} activation peaked early in SDp and started to gradually decline before the onset of SD, suggesting that it may provide some protection. Moreover, the greater abundance of T_{regs} in SDp presenting with OI than DHF/DSS also suggests that T_{regs} may protect from cytokine storm.

While most immune alterations in SDp largely resolved at convalescence, among the few that persisted were higher expression of PD-1 on T_{regs} and EM $CD4^+$ T cells and PD-L1 on NK cells. Sustained checkpoint protein expression may enhance immune regulation upon subsequent infection (*68*) and/or represent a preexisting immune set point altering dengue severity.

SD diagnosis based on the more recent 2009 WHO criteria includes evidence for OI, in addition to plasma leakage and bleeding (DHF/DSS) (*2*). Nevertheless, in part because of the limited number of SD cases, no prior studies have compared these conditions, and it remained unknown whether they represented a continuous disease spectrum or distinct syndromes with differing pathogenic mechanisms. We provide evidence that while largely overlapping, some differential responses between SDp presenting with DHF/DSS or OI exist. First, the abundance of cDC2s, which expressed higher CD64 in correlation with detected IgG and expressed lower CD209, was greater in OI than in DHF/DSS. It is tempting to speculate that cDC2s serve as Trojan horses for DENV, facilitating dissemination to organs and tissue injury. The expansion of T_{regs} in SDp was also driven by OI SDp, further supporting the hypothesis that reduced DENV clearance facilitating dissemination plays a role in this SD phenotype. Beyond viral dissemination, it was shown that CD8 T cell responses are implicated in liver injury in the setting of DENV infection (*69*). Intriguingly, cDC1s, which stimulate such $CD8^+$ T cell responses, were expanded in OI but not in DHF/DSS SDp. In contrast, plasma cell abundance and IgG usage were more prominent in DHF/DSS than in OI, suggesting that ADE and/or another mechanism, such as complement activation in response

to immune complex formation, may promote secretion of vasoactive products, leading to bleeding and/or shock (*70*, *71*). Production of vasoactive cytokines may be further augmented by the reduced T_{reg} expansion in DHF/DSS patients, in contrast to OI SDp (*62*). It will be important to monitor these responses in a larger number of SDp and in infections involving other organs beyond liver.

Evidence for NK cell activation in SDp was detected in the combined cohort, with SDp showing higher expression of Ki-67 and CD38, and in agreement with a former study, CD69, an activating receptor that contributes to sustained NK cell cytotoxicity, proliferation, and tumor necrosis factor–α (TNF-α) and adhesion molecule production (*45*, *72*). Nevertheless, comparing children and adult NK cell responses highlighted additional findings. On one hand, $CD56^{dim}CD16^{+}$ NK cells, which have known cytotoxic functions, showed evidence of increased activation in SDp children relative to SDp adults. First, the expression level of CD16 in SDp children was lower than in SDp adults. Since CD16 has been shown to be shed by metalloproteinases upon NK cell activation, thereby increasing NK cell survival and cytotoxicity via serial engagement of target cells (*73*), this finding suggests that these cells are activated. Thus, the predicted impact of this finding on clearance of DENV-infected cells is unclear. Second, $CD56^{dim}CD16^{+}$ NK cells in SDp children but not in adults expressed higher HLA-DR. HLA-DR expression on NK cells has been implicated in other disease models not only in proliferation, degranulation, and IFN-γ production but also in antigen presentation and activation of T cell responses (*36*, *37*). It is tempting to speculate that NK cells are activated, at least in part, to compensate for the lack of adequate T cell responses, thereby promoting viral clearance and protection.

On the other hand, it appears that in SDp, and particularly SDp children, such compensation may not be sufficient/effective, since the abundance of the $CD56^{dim}CD16^{+}$ NK cell population was reduced relative to D patients. This finding uncovers a potential reduction not only in NK cell–mediated killing of virally infected cells but also in NK cell homing to tissues (*74*–*76*). The concurrent expansion of cytokine-producing $CD56^{+}$ NK cells suggests that enhanced proinflammatory responses in SDp children relative to adults may further increase vascular permeability, more commonly reported in children (*20*).

Beyond altered NK cell responses, SDp children demonstrated greater reduction in HLA-DR expression on myeloid cell populations than SDp adults and a trend toward reduction of $CD16^{+}$ monocytes, suggesting a greater impairment in antigen presentation and possibly other monocyte functions. Moreover, $CD8^{+}$ TEMRA in SDp children, but not in SDp adults, expressed higher levels of HLA-DR. While there was no difference in checkpoint molecule expression on this cell type between disease severity categories, the increase in CD38 expression detected in children may suggest a more activated $CD8^{+}$ T cell response. In contrast, SDp adults showed a more prominent expansion of proliferating plasma cells expressing high levels of PD-L1 than SDp children. Together, these findings provide evidence that suppressed innate immune responses involved in cell killing and antigen presentation impairing viral clearance and increased activation of $CD8^{+}$ TEMRAs may predominate in SDp children, whereas plasma cell expansion predominates in SDp adults. While prior exposure to DENV was similar between SDp adults and children (73 versus 57%, respectively), it is possible that differences in the number of prior infections and/or time from last infection contribute to the differences in immune responses we detect between the two age groups.

A limitation of our study is that our cohort included more SDp females than males (16 versus 6). Since female gender and pregnancy are reported risk factors for SD progression (*22*, *77*), monitoring these responses in a gender-balanced cohort is important. We were also motivated to compare the immune response in SDp who had no prior exposure to DENV (primary infection), where ADE is unlikely to play a role, with secondarily infected SDp. Nevertheless, the number of definitive primary SDp was low (n = 2). Moreover, genetic background plays a role in SD pathogenesis, as evidenced by the lower incidence of SD progression in Africa (*78*). Therefore, probing the generalizability of our findings in other cohorts and identifying cell-specific generalizable signatures, as those we have recently identified in bulk samples (*7*, *8*), is also important. The lack of monitoring DENV-specific effector cell responses is another limitation of this study. Last, future studies are needed to monitor the host response following the mosquito bite and during the first 2 to 3 days of symptoms. Since difficult to capture in natural DENV infection, inoculation studies as those previously conducted (*79*, *80*) would be ideal for addressing this knowledge gap.

There is an urgent need for a prognostic assay to predict SD early in the disease course to improve patient triage and help select patients for therapeutic studies. We and others have recently identified candidate clinically usable biomarkers (*7*–*10*, *81*). However, additional biomarkers are needed until a prognostic assay is available and validated. Further studies in cohorts that include only samples obtained before the onset of SD are required to validate the changes in cell subtype abundance and/or marker expression that we identified as candidate predictive biomarkers. Such determinants may also serve as potential drug targets to prevent SD or treat it. While speculative, CD38 inhibitors (*33*, *82*) and CTLA-4 and PD-1 inhibitors (*83*) are a few examples for existing strategies that, based on our data, may modulate immune responses to favor viral clearance. Blockade of PD-1/PD-L1 interaction with a monoclonal antibody in PBMCs isolated from patients acutely infected with another Flaviviridae, hepatitis C virus, restored exhausted CD8 T cell responses, leading to increased T cell proliferation and cytokine production (*84*). Similar protection was observed in mice infected with influenza virus, where blockade of PD-L1 improved CD8 T cell function and enhanced recovery (*85*). Beyond further validation, functional characterization of these candidate biomarkers and therapeutic targets is required. In summary, this study provides insight into the pathogenesis of SD in natural infection in humans at a high resolution and proposes cellular and molecular determinants as candidate biomarkers associated with SD and/or targets for countermeasures to treat SD for further validation.

MATERIALS AND METHODS

Study population

PBMC samples were collected from individuals presenting to the Fundación Valle del Lili in Cali, Colombia or Centro de Atención y Diagnóstico de Enfermedades Infecciosas (CDI) in Bucamaranga between 2016 and 2019 with symptoms compatible with dengue, as previously described (*7*). All work with human subjects was approved by the Stanford University Administrative Panel on Human Subjects in Medical Research (protocol nos. 35460 and

50513) and the ethics committees in biomedical research of the Fundación Valle del Lili (Cali/Colombia) and the CDI (Bucaramanga/Colombia). All subjects, their parents, or legal guardians provided written informed consent, and subjects between 6 and 17 years of age and older provided assent.

PBMC isolation

PBMCs were isolated using SepMate tubes (STEMCELL Technologies) according to the manufacturer's instructions. Whole blood was diluted 1:1 with phosphate-buffered saline (PBS) and added to a SepMate tube, which contained 15 ml of Ficoll. Tubes were then centrifuged for 10 min at 1200*g*, after which the PBMC layer was poured off into a fresh tube and washed with PBS. Tubes were then centrifuged at 250*g* for 10 min and resuspended in freezing medium. Cryovials containing PBMCs were then placed in CoolCell at −80°C for 24 hours before being transferred to liquid nitrogen for storage. Samples were also shipped in liquid nitrogen.

Confirmation of dengue diagnosis

The confirmation of dengue diagnosis and screening for other arboviruses including Zika virus and chikungunya virus was performed as previously described (*8*). Briefly, serum samples were screened with a qualitative, single-reaction, multiplex real-time RT-PCR (rRT-PCR), which detects Zika, chikungunya, and DENV RNA (*86*). The DENV serotype and viral load were detected and quantitated using a separate DENV multiplex rRT-PCR (*87*).

Serologic and avidity testing was performed via a multiplexed antigen microarray containing DENV-2 whole virus particles spotted on pGOLD slides (Nirmidas Biotech, California), as described (*8*, *88*). Previously defined cutoffs based on mean levels +3 SDs were used.

Antibody conjugation and lyophilization

Antibody conjugation was performed as previously described (*89*). Briefly, metal isotope–labeled antibodies used in this study were conjugated using the MaxPar X8 antibody labeling kit per the manufacturer's instructions (Fluidigm) or purchased from Fluidigm preconjugated. Each conjugated antibody was quality checked and titrated to optimal staining concentration on healthy human PBMCs. Aliquots of the optimized surface and intracellular antibody cocktails and live cell barcoding (LCB) cocktails (*90*) were lyophilized to minimize batch effect, as previously described (*91*). Briefly, 20 μl of 500 mM trehalose in deionized, distilled water (DDW) was added to each aliquot, and the final volume of each aliquot was brought to 100 μl with DDW. Aliquots were transferred uncapped into a prechilled tube rack in a lidded cryobox (Biocision) and placed at −80°C for 1 hour. Aliquots were transferred to a vacuum chamber cabinet for 24 hours. Desiccated aliquots were kept at −20°C until reconstituted for cell staining.

Mass cytometry workflow

Samples were processed in eight batches of 20 samples. For each batch, an aliquot of a common cryopreserved PBMC sample from a healthy donor was added for batch correction. Cryopreserved PBMC samples where thawed at 37°C and transferred to 13 ml of cold cell culture medium [RPMI 1640 (Gibco), 10% fetal bovine serum, sodium heparin (20 U/ml), and benzonase (0.025 U/ml) (Sigma-Aldrich)] and washed once (250*g*, 4°C). After cell counting, up to 1.5 million cells per sample were transferred into new tubes and washed in cell-staining medium [CSM; PBS, 0.5% bovine serum albumin, and 0.02% sodium azide (Sigma-Aldrich); 250*g*, 4°C]. Cells were stained with LCB cocktails (reconstituted in CSM) for 30 min at 25°C. Cells were washed in CSM (250*g*, 4°C), Fc-blocked for 10 min (FcX, BioLegend), and stained with the surface antibody cocktail (reconstituted in CSM) for 60 min at 25°C. Viability staining was performed by resuspending cells in 1 ml of 500 nM PdCl in PBS for 5 min. Cells were washed in CSM (250*g*, 4°C) and fixed using the FoxP3/transcription factor fixation buffer (eBioscience) for 1 hour at 25°C. Cells were washed in FoxP3/transcription factor permeabilization buffer (eBioscience) (500*g*, 4°C) and stained with the intracellular antibody cocktail (reconstituted in permeabilization buffer) for 1 hour at 25°C. Cells were washed in permeabilization buffer (500*g*, 4°C) and resuspended in intercalator solution [PBS, 1.6% paraformaldehyde, and 0.5 mM rhodium (Fluidigm)] overnight at 4°C. The next day, cells were washed once in CSM and twice in DDW (500*g*, 4°C), filtered through a 35-mm nylon mesh cell strainer, and resuspended in DDW with 1× EQ four-element calibration beads (Fluidigm). Barcoded samples were acquired in several fcs files over the course of a day on a CyTOF2 mass cytometer (Fluidigm) using a Super Sampler injection system (Victorian Airship).

Data preprocessing

Fcs files from the mass cytometer were bead-normalized within each batch (*92*) using the R package, premessa, except for batch 6, which lacked sufficient bead events. Files were uploaded to cellengine.com, and leukocytes were gated as barium$^+$ DNA$^+$ bead$^-$ viability$^-$ and CD45$^+$ (fig. S1B) (*93*). Fcs files were downloaded and compensated with the R package, CATALYST (*94*). Files from batch 6 were 99th percentile normalized to account for sensitivity drift over time without bead normalization. Within each batch, CD3 was quantile normalized across files to account for antibody degradation over the course of acquisition (fig. S1C). Files within each batch were then concatenated and debarcoded using premessa. Fcs files with <1000 events were removed from downstream analysis. Fcs files were transformed with hyperbolic arcsin function using a cofactor of 5.

Batch correction was performed using the control sample included with each batch. For each protein channel, the median expression value was determined for all controls. The difference in medians was subtracted from all events to shift the distributions downward to have identical medians. Negative values that were introduced by this process were reset to the absolute value of a random normal distribution centered at zero to align with the noise floor for each channel. The resulting distributions were then 99th percentile normalized downward. The transforms applied to each batch control sample were then applied to all samples from that batch. This approach retained biological heterogeneity while accommodating batch correction for a range of distributions and batch effect manifestations (fig. S1D).

Clustering

Clustering was used to organize cells into known immune cell subsets rather than to find novel phenotypes. In this way, expression of activation molecules, checkpoint molecules, etc. that were not used for clustering could be compared between clinical groups without introducing bias. We used a supervised hierarchical clustering method that parallels manual gating, as previously described

(*95*). Briefly, cells were overclustered using the FlowSOM package (*96*), and clusters were manually assigned to cell type (T, B, NK, and myeloid) (Fig. 1B, panels). For each cell type, cells were reclustered with FlowSOM using only markers specific to that cell type (e.g., CD4 was used to cluster T cells, but not B cells). Clusters were then manually assigned to cell subtype (Fig. 1C, colors) and cell population (Fig. 1B, rows) based on known expression patterns (*89*, *93*, *95*, *97*).

Feature set generation

For each sample, summary statistics were derived, which were used for various comparisons. Samples with <3000 cells were removed from downstream analyses due to sampling bias. The proportions of cell populations out of total leukocytes and the proportion of cell populations out of cell subtypes were calculated. For B cells, the proportion of isotype usage and ratios of isotype usage were also calculated for each cell population. For each cell population, the mean expression of markers relevant to that cell type was quantified (e.g., CTLA-4 was quantified on T cells but not myeloid cells). Mean expression was chosen as changes in the mean are sensitive to both a shift in protein copy number and a shift in the percent of positive cells. Percent positive was not used as a feature due to high correlation with the mean.

Dimensionality reduction

The LDA (Fig. 1E) was generated with the MASS package using all features significantly different between any pairwise comparison of acute clinical status samples. The manifold was trained to separate samples by clinical status. The UMAP (Fig. 1C) was generated using the uwot package with min_dist = 0.7 and n_neighbors = 15, with all proteins as input and an equal subsampling of patients and clinical statuses. UMAP coordinates were initialized with LDA coordinates, trained to separate cell subtype (*25*).

Statistical analyses

All pairwise comparisons between samples used the Wilcoxon rank sum test for all features. For comparisons between acute samples, multiple hypothesis correction was performed using FDR. Features were only considered significantly different if $q < 0.05$ and $|\text{effect}| > 0.5$. For comparisons between convalescent samples, time points, children, adults, and SD subtypes, multiple hypothesis correction was not used because of small sample sizes. To maintain statistical rigor, the effect size requirement was increased, so features were only considered significant if $P < 0.05$ and $|\text{effect}| > 1.0$. For correlation analysis, the Pearson method was used and with multiple hypothesis correction using FDR when multiple correlations were calculated.

Supplementary Materials

This PDF file includes:
Supplementary Text
Figs. S1 to S7
Legends for tables S1 to S6
References

Other Supplementary Material for this manuscript includes the following:
Tables S1 to S6

REFERENCES AND NOTES

1. S. Bhatt, P. W. Gething, O. J. Brady, J. P. Messina, A. W. Farlow, C. L. Moyes, J. M. Drake, J. S. Brownstein, A. G. Hoen, O. Sankoh, M. F. Myers, D. B. George, T. Jaenisch, G. R. W. Wint, C. P. Simmons, T. W. Scott, J. J. Farrar, S. I. Hay, The global distribution and burden of dengue. *Nature* **496**, 504–507 (2013).
2. World Health Organization & UNICEF/UNDP/World Bank/WHO Special Programme for Research and Training in Tropical Diseases, *Handbook for Clinical Management of Dengue* (World Health Organization, 2012); https://apps.who.int/iris/handle/10665/76887.
3. J. D. Stanaway, D. S. Shepard, E. A. Undurraga, Y. A. Halasa, L. E. Coffeng, O. J. Brady, S. I. Hay, N. Bedi, I. M. Bensenor, C. A. Castañeda-Orjuela, T.-W. Chuang, K. B. Gibney, Z. A. Memish, A. Rafay, K. N. Ukwaja, N. Yonemoto, C. J. L. Murray, The global burden of dengue: An analysis from the Global Burden of Disease Study 2013. *Lancet Infect. Dis.* **16**, 712–723 (2016).
4. Z. Zeng, J. Zhan, L. Chen, H. Chen, S. Cheng, Global, regional, and national dengue burden from 1990 to 2017: A systematic analysis based on the global burden of disease study 2017. *EClinicalMedicine* **32**, 100712 (2021).
5. S. R. S. Hadinegoro, The revised WHO dengue case classification: Does the system need to be modified? *Paediatr. Int. Child Health.* **32**, 33–38 (2012).
6. F. Narvaez, G. Gutierrez, M. A. Pérez, D. Elizondo, A. Nuñez, A. Balmaseda, E. Harris, Evaluation of the traditional and revised WHO classifications of dengue disease severity. *PLOS Negl. Trop. Dis.* **5**, e1397 (2011).
7. Y. E. Liu, S. Saul, A. M. Rao, M. L. Robinson, O. L. Agudelo Rojas, A. M. Sanz, M. Verghese, D. Solis, M. Sibai, C. H. Huang, M. K. Sahoo, R. M. Gelvez, N. Bueno, M. I. Estupiñan Cardenas, L. A. Villar Centeno, E. M. Rojas Garrido, F. Rosso, M. Donato, B. A. Pinsky, S. Einav, P. Khatri, An 8-gene machine learning model improves clinical prediction of severe dengue progression. *Genome Med.* **14**, 33 (2022).
8. M. Robinson, T. E. Sweeney, R. Barouch-Bentov, M. K. Sahoo, L. Kalesinskas, F. Vallania, A. M. Sanz, E. Ortiz-Lasso, L. L. Albornoz, F. Rosso, J. G. Montoya, B. A. Pinsky, P. Khatri, S. Einav, A 20-gene set predictive of progression to severe dengue. *Cell Rep.* **26**, 1104–1111.e4 (2019).
9. H. Tissera, A. P. S. Rathore, W. Y. Leong, B. L. Pike, T. E. Warkentien, F. S. Farouk, A. Syenina, E. Eong Ooi, D. J. Gubler, A. Wilder-Smith, A. L. S. John, Chymase level is a predictive biomarker of dengue hemorrhagic fever in pediatric and adult patients. *J. Infect. Dis.* **216**, 1112–1121 (2017).
10. F. Zanini, M. L. Robinson, D. Croote, M. K. Sahoo, A. M. Sanz, E. Ortiz-Lasso, L. L. Albornoz, F. Rosso, J. G. Montoya, L. Goo, B. A. Pinsky, S. R. Quake, S. Einav, Virus-inclusive single-cell RNA sequencing reveals the molecular signature of progression to severe dengue. *Proc. Natl. Acad. Sci. U.S.A.* **115**, E12363–E12369 (2018).
11. S. Halstead, E. O'Rourke, Dengue viruses and mononuclear phagocytes. I. Infection enhancement by non-neutralizing antibody. *J. Exp. Med.* **146**, 201–217 (1977).
12. S. B. Halstead, E. J. O'rourke, Antibody-enhanced dengue virus infection in primate leukocytes. *Nature* **265**, 739–741 (1977).
13. L. C. Katzelnick, L. Gresh, M. E. Halloran, J. C. Mercado, G. Kuan, A. Gordon, A. Balmaseda, E. Harris, Antibody-dependent enhancement of severe dengue disease in humans. *Science* **358**, 929–932 (2017).
14. M. Kwissa, H. I. Nakaya, N. Onlamoon, J. Wrammert, F. Villinger, G. C. Perng, S. Yoksan, K. Pattanapanyasat, K. Chokephaibulkit, R. Ahmed, B. Pulendran, Dengue virus infection induces expansion of a $CD14^{+}CD16^{+}$ monocyte population that stimulates plasmablast differentiation. *Cell Host Microbe* **16**, 115–127 (2014).
15. E. J. M. Nascimento, E. D. Hottz, T. M. Garcia-Bates, F. Bozza, E. T. A. Marques, S. M. Barratt-Boyes, Emerging concepts in dengue pathogenesis: Interplay between plasmablasts, platelets, and complement in triggering vasculopathy. *Crit. Rev. Immunol.* **34**, 227–240 (2014).
16. J. Mongkolsapaya, T. Duangchinda, W. Dejnirattisai, S. Vasanawathana, P. Avirutnan, A. Jairungsri, N. Khemnu, N. Tangthawornchaikul, P. Chotiyarnwong, K. Sae-Jang, M. Koch, Y. Jones, A. McMichael, X. Xu, P. Malasit, G. Screaton, T cell responses in dengue hemorrhagic fever: Are cross-reactive T cells suboptimal? *J. Immunol.* **176**, 3821–3829 (2006).
17. S.-T. Chen, Y.-L. Lin, M.-T. Huang, M.-F. Wu, S.-C. Cheng, H.-Y. Lei, C.-K. Lee, T.-W. Chiou, C.-H. Wong, S.-L. Hsieh, CLEC5A is critical for dengue-virus-induced lethal disease. *Nature* **453**, 672–676 (2008).
18. W.-K. Wang, H.-L. Chen, C.-F. Yang, S.-C. Hsieh, C.-C. Juan, S.-M. Chang, C.-C. Yu, L.-H. Lin, J.-H. Huang, C.-C. King, Slower rates of clearance of viral load and virus-containing immune complexes in patients with dengue hemorrhagic fever. *Clin. Infect. Dis.* **43**, 1023–1030 (2006).
19. D. W. Vaughn, S. Green, S. Kalayanarooj, B. L. Innis, S. Nimmannitya, S. Suntayakorn, T. P. Endy, B. Raengsakulrach, A. L. Rothman, F. A. Ennis, A. Nisalak, Dengue viremia titer, antibody response pattern, and virus serotype correlate with disease severity. *J. Infect. Dis.* **181**, 2–9 (2000).

20. M. G. Guzmán, G. Kouri, J. Bravo, L. Valdes, S. Vazquez, S. B. Halstead, Effect of age on outcome of secondary dengue 2 infections. *Int. J. Infect. Dis.* **6**, 118–124 (2002).
21. O. Wichmann, S. Hongsiriwon, C. Bowonwatanuwong, K. Chotivanich, Y. Sukthana, S. Pukrittayakamee, Risk factors and clinical features associated with severe dengue infection in adults and children during the 2001 epidemic in Chonburi, Thailand. *Trop. Med. Int. Health* **9**, 1022–1029 (2004).
22. S. Sangkaew, D. Ming, A. Boonyasiri, K. Honeyford, S. Kalayanarooj, S. Yacoub, I. Dorigatti, A. Holmes, Risk predictors of progression to severe disease during the febrile phase of dengue: A systematic review and meta-analysis. *Lancet Infect. Dis.* **21**, 1014–1026 (2021).
23. A. Karunakaran, W. M. Ilyas, S. F. Sheen, N. K. Jose, Z. T. Nujum, Risk factors of mortality among dengue patients admitted to a tertiary care setting in Kerala, India. *J. Infect. Public Health* **7**, 114–120 (2014).
24. E. Becht, L. McInnes, J. Healy, C.-A. Dutertre, I. W. H. Kwok, L. G. Ng, F. Ginhoux, E. W. Newell, Dimensionality reduction for visualizing single-cell data using UMAP. *Nat. Biotechnol.* **37**, 38–44 (2019).
25. M. Amouzgar, D. R. Glass, R. Baskar, I. Averbukh, S. C. Kimmey, A. G. Tsai, F. J. Hartmann, S. C. Bendall, Supervised dimensionality reduction for exploration of single-cell data by HSS-LDA. *Patterns (N Y)* **3**, 100536 (2022).
26. L. A. Callender, E. C. Carroll, R. W. J. Beal, E. S. Chambers, S. Nourshargh, A. N. Akbar, S. M. Henson, Human $CD8^+$ EMRA T cells display a senescence-associated secretory phenotype regulated by p38 MAPK. *Aging Cell* **17**, e12675 (2018).
27. M. Collin, V. Bigley, Human dendritic cell subsets: An update. *Immunology* **154**, 3–20 (2018).
28. M. Gilliet, W. Cao, Y.-J. Liu, Plasmacytoid dendritic cells: Sensing nucleic acids in viral infection and autoimmune diseases. *Nat. Rev. Immunol.* **8**, 594–606 (2008).
29. J. K. Krishnaswamy, U. Gowthaman, B. Zhang, J. Mattsson, L. Szeponik, D. Liu, R. Wu, T. White, S. Calabro, L. Xu, M. A. Collet, M. Yurieva, S. Alsén, P. Fogelstrand, A. Walter, W. R. Heath, S. N. Mueller, U. Yrlid, A. Williams, S. C. Eisenbarth, Migratory $CD11b^+$ conventional dendritic cells induce T follicular helper cell-dependent antibody responses. *Sci. Immunol.* **2**, eaam9169 (2017).
30. S. Bournazos, A. Gupta, J. V. Ravetch, The role of IgG Fc receptors in antibody-dependent enhancement. *Nat. Rev. Immunol.* **20**, 633–643 (2020).
31. K. A. Hogan, C. C. S. Chini, E. N. Chini, The multi-faceted ecto-enzyme CD38: Roles in immunomodulation, cancer, aging, and metabolic diseases. *Front. Immunol.* **10**, 1187 (2019).
32. E. I. Buchbinder, A. Desai, CTLA-4 and PD-1 pathways. *Am. J. Clin. Oncol.* **39**, 98–106 (2016).
33. X. Feng, L. Zhang, C. Acharya, G. An, K. Wen, L. Qiu, N. Munshi, Y.-T. Tai, K. C. Anderson, Targeting CD38 suppresses induction and function of T regulatory cells to mitigate immunosuppression in multiple myeloma. *Clin. Cancer Res.* **23**, 4290–4300 (2017).
34. Y.-H. Li, C.-H. Kuo, G.-Y. Shi, H.-L. Wu, The role of thrombomodulin lectin-like domain in inflammation. *J. Biomed. Sci.* **19**, 34 (2012).
35. B. Tassaneetrithep, T. H. Burgess, A. Granelli-Piperno, C. Trumpfheller, J. Finke, W. Sun, M. A. Eller, K. Pattanapanyasat, S. Sarasombath, D. L. Birx, R. M. Steinman, S. Schlesinger, M. A. Marovich, DC-SIGN (CD209) mediates dengue virus infection of human dendritic cells. *J. Exp. Med.* **197**, 823–829 (2003).
36. S. A. Erokhina, M. A. Streltsova, L. M. Kanevskiy, W. G. Telford, A. M. Sapozhnikov, E. I. Kovalenko, $HLA\text{-}DR^+$ NK cells are mostly characterized by less mature phenotype and high functional activity. *Immunol. Cell Biol.* **96**, 212–228 (2018).
37. S. A. Kust, M. A. Streltsova, A. V. Panteleev, N. L. Karpina, I. V. Lyadova, A. M. Sapozhnikov, E. I. Kovalenko, HLA-DR-positive NK cells expand in response to mycobacterium tuberculosis antigens and mediate mycobacteria-induced T cell activation. *Front. Immunol.* **12**, 662128 (2021).
38. D. G. Schatz, Y. Ji, Recombination centres and the orchestration of V(D)J recombination. *Nat. Rev. Immunol.* **11**, 251–263 (2011).
39. P. Bruhns, B. Iannascoli, P. England, D. A. Mancardi, N. Fernandez, S. Jorieux, M. Daëron, Specificity and affinity of human Fcγ receptors and their polymorphic variants for human IgG subclasses. *Blood* **113**, 3716–3725 (2009).
40. T. T. Wang, J. Sewatanon, M. J. Memoli, J. Wrammert, S. Bournazos, S. K. Bhaumik, B. A. Pinsky, K. Chokephaibulkit, N. Onlamoon, K. Pattanapanyasat, J. K. Taubenberger, R. Ahmed, J. V. Ravetch, IgG antibodies to dengue enhanced for FcγRIIIA binding determine disease severity. *Science* **355**, 395–398 (2017).
41. S. J. Balsitis, J. Coloma, G. Castro, A. Alava, D. Flores, J. H. McKerrow, P. R. Beatty, E. Harris, Tropism of dengue virus in mice and humans defined by viral nonstructural protein 3-specific immunostaining. *Am. J. Trop. Med. Hyg.* **80**, 416–424 (2009).
42. S. N. Hammond, A. Balmaseda, L. Pérez, Y. Tellez, S. I. Saborío, J. C. Mercado, E. Videa, Y. Rodriguez, M. A. Pérez, R. Cuadra, S. Solano, J. Rocha, W. Idiaquez, A. Gonzalez, E. Harris, Differences in dengue severity in infants, children, and adults in a 3-year hospital-based study in Nicaragua. *Am. J. Trop. Med. Hyg.* **73**, 1063–1070 (2005).
43. K. Srpan, A. Ambrose, A. Karampatzakis, M. Saeed, A. N. R. Cartwright, K. Guldevall, G. D. S. C. De Matos, B. Önfelt, D. M. Davis, Shedding of CD16 disassembles the NK cell immune synapse and boosts serial engagement of target cells. *J. Cell Biol.* **217**, 3267–3283 (2018).
44. G. Peruzzi, L. Femnou, A. Gil-Krzewska, F. Borrego, J. Weck, K. Krzewski, J. E. Coligan, Membrane-type 6 matrix metalloproteinase regulates the activation-induced downmodulation of CD16 in human primary NK cells. *J. Immunol.* **191**, 1883–1894 (2013).
45. F. Borrego, M. J. Robertson, J. Ritz, J. Peña, R. Solana, CD69 is a stimulatory receptor for natural killer cell and its cytotoxic effect is blocked by CD94 inhibitory receptor. *Immunology* **97**, 159–165 (1999).
46. M. C. Glass, D. R. Glass, J.-P. Oliveria, B. Mbiribindi, C. O. Esquivel, S. M. Krams, S. C. Bendall, O. M. Martinez, Human IL-10-producing B cells have diverse states that are induced from multiple B cell subsets. *Cell Rep.* **39**, 110728 (2022).
47. Y. Zhao, M. Amodio, B. V. Wyk, B. Gerritsen, M. M. Kumar, D. van Dijk, K. Moon, X. Wang, A. Malawista, M. M. Richards, M. E. Cahill, A. Desai, J. Sivadasan, M. M. Venkataswamy, V. Ravi, E. Fikrig, P. Kumar, S. H. Kleinstein, S. Krishnaswamy, R. R. Montgomery, Single cell immune profiling of dengue virus patients reveals intact immune responses to Zika virus with enrichment of innate immune signatures. *PLOS Negl. Trop. Dis.* **14**, e0008112 (2020).
48. R. Fenutria, K. Maringer, U. Potla, D. Bernal-Rubio, M. J. Evans, E. Harris, A. H. Rahman, A. Fernandez-Sesma, I. Ramos, CyTOF profiling of Zika and dengue virus-infected human peripheral blood mononuclear cells identifies phenotypic signatures of monotype subsets and upregulation of the interferon-inducible protein CD169. *mSphere* **6**, e0050521 (2021).
49. A. Rouers, M. H. Y. Chng, B. Lee, M. P. Rajapakse, K. Kaur, Y. X. Toh, D. Sathiakumar, T. Loy, T.-L. Thein, V. W. X. Lim, A. Singhal, T. W. Yeo, Y.-S. Leo, K. A. Vora, D. Casimiro, B. Lim, L. Tucker-Kellogg, L. Rivino, E. W. Newell, K. Fink, Immune cell phenotypes associated with disease severity and long-term neutralizing antibody titers after natural dengue virus infection. *Cell Rep. Med.* **2**, 100278 (2021).
50. R. Appanna, S. Kg, M. H. Xu, Y.-X. Toh, S. Velumani, D. Carbajo, C. Y. Lee, R. Zuest, T. Balakrishnan, W. Xu, B. Lee, M. Poidinger, F. Zolezzi, Y. S. Leo, T. L. Thein, C.-I. Wang, K. Fink, Plasmablasts during acute dengue infection represent a small subset of a broader virus-specific memory B cell pool. *EBioMedicine* **12**, 178–188 (2016).
51. A. L. Rothman, Immunity to dengue virus: A tale of original antigenic sin and tropical cytokine storms. *Nat. Rev. Immunol.* **11**, 532–543 (2011).
52. K. Buscher, P. Marcovecchio, C. C. Hedrick, K. Ley, Patrolling mechanics of non-classical monocytes in vascular inflammation. *Front. Cardiovasc. Med.* **4**, 80 (2017).
53. S. A. Marsh, H. M. Arthur, I. Spyridopoulos, The secret life of nonclassical monocytes. *Cytometry A* **91**, 1055–1058 (2017).
54. D. Maheshwari, K. Saini, P. Singh, M. Singla, K. Nayak, C. Aggarwal, Y. M. Chawla, P. Bajpai, M. Kaur, S. Gunisetty, C. S. Eberhardt, R. Nyodu, K. Moore, M. S. Suthar, G. R. Medigeshi, E. Anderson, R. Lodha, S. K. Kabra, R. Ahmed, A. Chandele, K. Murali-Krishna, Contrasting behavior between the three human monocyte subsets in dengue pathophysiology. *iScience* **25**, 104384 (2022).
55. T. Chawla, K. R. Chan, S. L. Zhang, H. C. Tan, A. P. C. Lim, B. J. Hanson, E. E. Ooi, Dengue virus neutralization in cells expressing Fc gamma receptors. *PLOS ONE* **8**, e65231 (2013).
56. W. W. S. I. Rodrigo, O. K. T. Block, C. Lane, S. Sukupolvi-Petty, A. P. Goncalvez, S. Johnson, M. S. Diamond, C.-J. Lai, R. C. Rose, X. Jin, J. J. Schlesinger, Dengue virus neutralization is modulated by IgG antibody subclass and Fcγ receptor subtype. *Virology* **394**, 175–182 (2009).
57. A. Silvin, C. I. Yu, X. Lahaye, F. Imperatore, J.-B. Brault, S. Cardinaud, C. Becker, W.-H. Kwan, C. Conrad, M. Maurin, C. Goudot, S. Marques-Ladeira, Y. Wang, V. Pascual, E. Anguiano, R. A. Albrecht, M. Iannacone, A. García-Sastre, B. Goud, M. Dalod, A. Moris, M. Merad, A. K. Palucka, N. Manel, Constitutive resistance to viral infection in human $CD141^+$ dendritic cells. *Sci. Immunol.* **2**, eaai8071 (2017).
58. C.-C. Chu, N. Ali, P. Karagiannis, P. Di Meglio, A. Skowera, L. Napolitano, G. Barinaga, K. Grys, E. Sharif-Paghaleh, S. N. Karagiannis, M. Peakman, G. Lombardi, F. O. Nestle, Resident $CD141\ (BDCA3)^+$ dendritic cells in human skin produce IL-10 and induce regulatory T cells that suppress skin inflammation. *J. Exp. Med.* **209**, 935–945 (2012).
59. N. van Leeuwen-Kerkhoff, T. M. Westers, P. J. Poddighe, T. D. de Gruijl, S. Kordasti, A. A. van de Loosdrecht, Thrombomodulin-expressing monocytes are associated with low-risk features in myelodysplastic syndromes and dampen excessive immune activation. *Haematologica* **105**, 961–971 (2020).
60. J. P. Ren, J. Zhao, J. Dai, J. W. D. Griffin, L. Wang, X. Y. Wu, Z. D. Morrison, G. Y. Li, M. El Gazzar, S. B. Ning, J. P. Moorman, Z. Q. Yao, Hepatitis C virus-induced myeloid-derived suppressor cells regulate T-cell differentiation and function via the signal transducer and activator of transcription 3 pathway. *Immunology* **148**, 377–386 (2016).
61. L. Wang, J. Zhao, J. P. Ren, X. Y. Wu, Z. D. Morrison, M. A. Elgazzar, S. B. Ning, J. P. Moorman, Z. Q. Yao, Expansion of myeloid-derived suppressor cells promotes differentiation of regulatory T cells in $HIV\text{-}1^+$ individuals. *AIDS* **30**, 1521–1531 (2016).

62. K. Lühn, C. P. Simmons, E. Moran, N. T. P. Dung, T. N. B. Chau, N. T. H. Quyen, L. T. T. Thao, T. Van Ngoc, N. M. Dung, B. Wills, J. Farrar, A. J. McMichael, T. Dong, S. Rowland-Jones, Increased frequencies of $CD4^+CD25^{high}$ regulatory T cells in acute dengue infection. *J. Exp. Med.* **204**, 979–985 (2007).
63. H. E. Jayaratne, D. Wijeratne, S. Fernando, A. Kamaladasa, L. Gomes, A. Wijewickrama, G. S. Ogg, G. N. Malavige, Regulatory T-cells in acute dengue viral infection. *Immunology* **154**, 89–97 (2018).
64. P. Pandiyan, L. Zheng, S. Ishihara, J. Reed, M. J. Lenardo, $CD4^+CD25^+Foxp3^+$ regulatory T cells induce cytokine deprivation-mediated apoptosis of effector $CD4^+$ T cells. *Nat. Immunol.* **8**, 1353–1362 (2007).
65. W. Pierson, B. Cauwe, A. Policheni, S. M. Schlenner, D. Franckaert, J. Berges, S. Humblet-Baron, S. Schonefeldt, M. J. Herold, D. Hildeman, A. Strasser, P. Bouillet, L.-F. Lu, P. Matthys, A. A. Freitas, R. J. Luther, C. T. Weaver, J. Dooley, D. H. D. Gray, A. Liston, Anti-apoptotic Mcl-1 is critical for the survival and niche-filling capacity of $Foxp3^+$ regulatory T cells. *Nat. Immunol.* **14**, 959–965 (2013).
66. P. Ruibal, L. Oestereich, A. Lüdtke, B. Becker-Ziaja, D. M. Wozniak, R. Kerber, M. Korva, M. Cabeza-Cabrerizo, J. A. Bore, F. R. Koundouno, S. Duraffour, R. Weller, A. Thorenz, E. Cimini, D. Viola, C. Agrati, J. Repits, B. Afrough, L. A. Cowley, D. Ngabo, J. Hinzmann, M. Mertens, I. Vitoriano, C. H. Logue, J. P. Boettcher, E. Pallasch, A. Sachse, A. Bah, K. Nitzsche, E. Kuisma, J. Michel, T. Holm, E.-G. Zekeng, I. García-Dorival, R. Wölfel, K. Stoecker, E. Fleischmann, T. Strecker, A. Di Caro, T. Avšič-Županc, A. Kurth, S. Meschi, S. Mély, E. Newman, A. Bocquin, Z. Kis, A. Kelterbaum, P. Molkenthin, F. Carletti, J. Portmann, S. Wolff, C. Castilletti, G. Schudt, A. Fizet, L. J. Ottowell, E. Herker, T. Jacobs, B. Kretschmer, E. Severi, N. Ouedraogo, M. Lago, A. Negredo, L. Franco, P. Anda, S. Schmiedel, B. Kreuels, D. Wichmann, M. M. Addo, A. W. Lohse, H. De Clerck, C. Nanclares, S. Jonckheere, M. Van Herp, A. Sprecher, G. Xiaojiang, M. Carrington, O. Miranda, C. M. Castro, M. Gabriel, P. Drury, P. Formenty, B. Diallo, L. Koivogui, N. Magassouba, M. W. Carroll, S. Günther, C. Muñoz-Fontela, Unique human immune signature of Ebola virus disease in Guinea. *Nature* **533**, 100–104 (2016).
67. R.-F. Chen, L. Wang, J.-T. Cheng, H. Chuang, J.-C. Chang, J.-W. Liu, I.-C. Lin, K. D. Yang, Combination of CTLA-4 and TGFβ1 gene polymorphisms associated with dengue hemorrhagic fever and virus load in a dengue-2 outbreak. *Clin. Immunol.* **131**, 404–409 (2009).
68. E. Simon-Lorière, V. Duong, A. Tawfik, S. Ung, S. Ly, I. Casadémont, M. Prot, N. Courtejoie, K. Bleakley, P. Buchy, A. Tarantola, P. Dussart, T. Cantaert, A. Sakuntabhai, Increased adaptive immune responses and proper feedback regulation protect against clinical dengue. *Sci. Transl. Med.* **9**, eaal5088 (2017).
69. J.-M. Sung, C.-K. Lee, B. A. Wu-Hsieh, Intrahepatic infiltrating NK and CD8 T cells cause liver cell death in different phases of dengue virus infection. *PLOS ONE* **7**, e46292 (2012).
70. D. Ricklin, J. D. Lambris, Complement in immune and inflammatory disorders: Pathophysiological mechanisms. *J. Immunol.* **190**, 3831–3838 (2013).
71. M. Xu, V. Hadinoto, R. Appanna, K. Joensson, Y. X. Toh, T. Balakrishnan, S. H. Ong, L. Warter, Y. S. Leo, C.-I. Wang, K. Fink, Plasmablasts generated during repeated dengue infection are virus glycoprotein-specific and bind to multiple virus serotypes. *J. Immunol.* **189**, 5877–5885 (2012).
72. S. Green, S. Pichyangkul, D. W. Vaughn, S. Kalayanarooj, S. Nimmannitya, A. Nisalak, I. Kurane, A. L. Rothman, F. A. Ennis, Early CD69 expression on peripheral blood lymphocytes from children with dengue hemorrhagic fever. *J. Infect. Dis.* **180**, 1429–1435 (1999).
73. R. Romee, B. Foley, T. Lenvik, Y. Wang, B. Zhang, D. Ankarlo, X. Luo, S. Cooley, M. Verneris, B. Walcheck, J. Miller, NK cell CD16 surface expression and function is regulated by a disintegrin and metalloprotease-17 (ADAM17). *Blood* **121**, 3599–3608 (2013).
74. V. Béziat, D. Duffy, S. N. Quoc, M. Le Garff-Tavernier, J. Decocq, B. Combadière, P. Debré, V. Vieillard, $CD56^{bright}CD16^+$ NK cells: A functional intermediate stage of NK cell differentiation. *J. Immunol.* **186**, 6753–6761 (2011).
75. R. Castriconi, P. Carrega, A. Dondero, F. Bellora, B. Casu, S. Regis, G. Ferlazzo, C. Bottino, Molecular mechanisms directing migration and retention of natural killer cells in human tissues. *Front. Immunol.* **9**, 2324 (2018).
76. C. L. Zimmer, M. Cornillet, C. Solà-Riera, K.-W. Cheung, M. A. Ivarsson, M. Q. Lim, N. Marquardt, Y.-S. Leo, D. C. Lye, J. Klingström, P. A. MacAry, H.-G. Ljunggren, L. Rivino, N. K. Björkström, NK cells are activated and primed for skin-homing during acute dengue virus infection in humans. *Nat. Commun.* **10**, 3897 (2019).
77. C. R. Machado, E. S. Machado, R. D. Rohloff, M. Azevedo, D. P. Campos, R. B. de Oliveira, P. Brasil, Is pregnancy associated with severe dengue? A review of data from the Rio de Janeiro surveillance information system. *PLOS Negl. Trop. Dis.* **7**, e2217 (2013).
78. E. M. Gainor, E. Harris, A. D. LaBeaud, Uncovering the burden of dengue in Africa: Considerations on magnitude, misdiagnosis, and sncestry. *Viruses* **14**, 233 (2022).
79. B. D. Kirkpatrick, S. S. Whitehead, K. K. Pierce, C. M. Tibery, P. L. Grier, N. A. Hynes, C. J. Larsson, B. P. Sabundayo, K. R. Talaat, A. Janiak, M. P. Carmolli, C. J. Luke, S. A. Diehl, A. P. Durbin, The live attenuated dengue vaccine TV003 elicits complete protection against dengue in a human challenge model. *Sci. Transl. Med.* **8**, 330ra36 (2016).
80. A. T. Waickman, K. Newell, J. Q. Lu, H. Fang, M. Waldran, C. Gebo, J. R. Currier, H. Friberg, R. G. Jarman, M. D. Klick, L. A. Ware, T. P. Endy, S. J. Thomas, Virologic, clinical, and immunological characteristics of a dengue virus 3 human challenge model. medrxiv 2022.10.24.22281454 (2022). https://doi.org/10.1101/2022.10.24.22281454.
81. S. Bournazos, H. T. M. Vo, V. Duong, H. Auerswald, S. Ly, A. Sakuntabhai, P. Dussart, T. Cantaert, J. V. Ravetch, Antibody fucosylation predicts disease severity in secondary dengue infection. *Science* **372**, 1102–1105 (2021).
82. A. Mauriello, C. Manolio, B. Cavalluzzo, A. Avallone, M. Borrelli, A. Morabito, E. Iovine, A. Chambery, R. Russo, M. L. Tornesello, F. M. Buonaguro, M. Tagliamonte, L. Buonaguro, Immunological effects of adjuvants in subsets of antigen presenting cells of cancer patients undergoing chemotherapy. *J. Transl. Med.* **18**, 34 (2020).
83. M. N. Wykes, S. R. Lewin, Immune checkpoint blockade in infectious diseases. *Nat. Rev. Immunol.* **18**, 91–104 (2018).
84. S. Urbani, B. Amadei, D. Tola, M. Massari, S. Schivazappa, G. Missale, C. Ferrari, PD-1 expression in acute hepatitis C virus (HCV) infection is associated with HCV-specific CD8 exhaustion. *J. Virol.* **80**, 11398–11403 (2006).
85. B. McNally, F. Ye, M. Willette, E. Flaño, Local blockade of epithelial PDL-1 in the airways enhances T cell function and viral clearance during influenza virus infection. *J. Virol.* **87**, 12916–12924 (2013).
86. J. J. Waggoner, L. Gresh, A. Mohamed-Hadley, G. Ballesteros, M. J. V. Davila, Y. Tellez, M. K. Sahoo, A. Balmaseda, E. Harris, B. A. Pinsky, Single-reaction multiplex reverse transcription PCR for detection of Zika, chikungunya, and dengue viruses. *Emerg. Infect. Dis.* **22**, 1295–1297 (2016).
87. J. J. Waggoner, J. Abeynayake, M. K. Sahoo, L. Gresh, Y. Tellez, K. Gonzalez, G. Ballesteros, A. M. Pierro, P. Gaibani, F. P. Guo, V. Sambri, A. Balmaseda, K. Karunaratne, E. Harris, B. A. Pinsky, Single-reaction, multiplex, real-time RT-PCR for the detection, quantitation, and serotyping of dengue viruses. *PLOS Negl. Trop. Dis.* **7**, e2116 (2013).
88. B. Zhang, B. A. Pinsky, J. S. Ananta, S. Zhao, S. Arulkumar, H. Wan, M. K. Sahoo, J. Abeynayake, J. J. Waggoner, C. Hopes, M. Tang, H. Dai, Diagnosis of Zika virus infection on a nanotechnology platform. *Nat. Med.* **23**, 548–550 (2017).
89. F. J. Hartmann, J. Babdor, P. F. Gherardini, E.-A. D. Amir, K. Jones, B. Sahaf, D. M. Marquez, P. Krutzik, E. O'Donnell, N. Sigal, H. T. Maecker, E. Meyer, M. H. Spitzer, S. C. Bendall, Comprehensive immune monitoring of clinical trials to advance human immunotherapy. *Cell Rep.* **28**, 819–831.e4 (2019).
90. F. J. Hartmann, E. F. Simonds, S. C. Bendall, A universal live cell barcoding-platform for multiplexed human single cell analysis. *Sci. Rep.* **8**, 10770 (2018).
91. B. Sahaf, A. Rahman, H. T. Maecker, S. Bendall, High-parameter immune profiling with CyTOF. *Methods Mol. Biol.* **2055**, 351–368 (2020).
92. R. Finck, E. F. Simonds, A. Jager, S. Krishnaswamy, K. Sachs, W. Fantl, D. Pe'er, G. P. Nolan, S. C. Bendall, Normalization of mass cytometry data with bead standards. *Cytometry A* **83**, 483–494 (2013).
93. A. G. Tsai, D. R. Glass, M. Juntilla, F. J. Hartmann, J. S. Oak, S. Fernandez-Pol, R. S. Ohgami, S. C. Bendall, Multiplexed single-cell morphometry for hematopathology diagnostics. *Nat. Med.* **26**, 408–417 (2020).
94. S. Chevrier, H. L. Crowell, V. R. T. Zanotelli, S. Engler, M. D. Robinson, B. Bodenmiller, Compensation of signal spillover in suspension and imaging mass cytometry. *Cell Syst.* **6**, 612–620.e5 (2018).
95. D. R. Glass, A. G. Tsai, J. P. Oliveria, F. J. Hartmann, S. C. Kimmey, A. A. Calderon, L. Borges, M. C. Glass, L. E. Wagar, M. M. Davis, S. C. Bendall, An integrated multi-omic single-cell atlas of human B cell identity. *Immunity* **53**, 217–232.e5 (2020).
96. S. Van Gassen, B. Callebaut, M. J. Van Helden, B. N. Lambrecht, P. Demeester, T. Dhaene, Y. Saeys, FlowSOM: Using self-organizing maps for visualization and interpretation of cytometry data. *Cytometry A* **87**, 636–645 (2015).
97. M. Alcántara-Hernández, R. Leylek, L. E. Wagar, E. G. Engleman, T. Keler, M. P. Marinkovich, M. M. Davis, G. P. Nolan, J. Idoyaga, High-dimensional phenotypic mapping of human dendritic cells reveals interindividual variation and tissue specialization. *Immunity* **47**, 1037–1050.e6 (2017).
98. A. P. Durbin, M. J. Vargas, K. Wanionek, S. N. Hammond, A. Gordon, C. Rocha, A. Balmaseda, E. Harris, Phenotyping of peripheral blood mononuclear cells during acute dengue illness demonstrates infection and increased activation of monocytes in severe cases compared to classic dengue fever. *Virology* **376**, 429–435 (2008).
99. J. L. Kyle, P. R. Beatty, E. Harris, Dengue virus infects macrophages and dendritic cells in a mouse model of infection. *J. Infect. Dis.* **195**, 1808–1817 (2007).
100. V. Upasani, H. T. M. Vo, H. Auerswald, D. Laurent, S. Heng, V. Duong, I. A. Rodenhuis-Zybert, P. Dussart, T. Cantaert, Direct infection of B cells by dengue virus modulates B cell responses in a Cambodian pediatric cohort. *Front. Immunol.* **11**, 594813 (2021).

Acknowledgments

Funding: This work was supported by Catalyst and Transformational Awards from Dr. Ralph & Marian Falk Medical Research Trust, Investigator Initiated Award number W81XWH1910235 from the Department of Defense (DoD) office of the Congressionally Directed Medical Research Programs (CDMRP)/Peer Reviewed Medical Research Program (PRMRP), and a National Institute of Allergy and Infectious Diseases (NIAID) grant U19 AI057229 supplement to S.E. S.E. is a Chan Zuckerberg Biohub investigator, who is also supported by Investigator Initiated Award number W81XWH2210283 and expansion award number W81XWH2110456 from the DoD office of the CDMRP/PRMRP, NIAID grant RO1AI158569, and Defense Threat Reduction Fundamental Research to Counter Weapons of Mass Destruction grant HDTRA11810039. M.L.R. was supported by the A.P. Giannini Foundation Postdoctoral Fellowship and the Harold Amos Medical Faculty Development Program. D.R.G. was supported by a Stanford Graduate Fellowship and a Bio-X Stanford Interdisciplinary Graduate Fellowship. V.D. was supported by a Chan Zuckerberg Biohub Collaborative Postdoctoral Fellowship. F.J.H. was supported by EMBO Long-Term Fellowship ALTF 1141–2017, Novartis Foundation for Medical-Biological Research 16C148, and Swiss National Science Foundation SNF Early Postdoc Mobility P2ZHP3-171741. S.C.B. was supported by NIH awards DP2EB024246, U24CA224309, R01AG057915, R01AG056287, R01AG068279, and 1UH3CA246633. The funders had no role in study design, data collection and analysis, decision to publish, or preparation of the manuscript. **Author contributions:** Conceptualization: S.E., M.L.R., and V.D. Methodology: D.R.G., M.L.R., S.C.B., M.K.S., B.A.P., H.M., and S.E. Software: D.R.G. and M.L.R. Formal analysis: D.R.G. and M.L.R. Investigation: M.L.R., D.R.G., V.D., F.J.H., and M.B. Resources: S.E., S.C.B., O.L.A.R., A.M.S., M.C., R.M.G., N.B., J.G.M., M.I.E.C., L.A.V.C., E.M.R.G., and F.R. Data curation: M.L.R., D.R.G., O.L.A.R., A.M.S., M.C., R.M.G., N.B., M.I.E.C., L.A.V.C., E.M.R.G., and F.R. Writing—original draft: M.L.R., D.R.G., and S.E. Writing—review and editing: M.L.R., D.R.G., S.E., V.D., and S.C.B. Visualization: D.R.G., M.L.R., and V.D. Supervision: S.E. and S.C.B. Funding acquisition: S.E. and S.C.B. **Competing interests:** The authors declare that they have no competing interests. **Data and materials availability:** All data needed to evaluate the conclusions in the paper are present in the paper and/or the Supplementary Materials. Fcs files can be accessed at FlowRepository: https://flowrepository.org/id/FR-FCM-Z5MQ, ID FR-FCM-Z5MQ. The processed data and code to reproduce figures can be accessed at: https://doi.org/10.5281/zenodo.7579634.

Submitted 6 September 2022
Accepted 21 February 2023
Published 24 March 2023
10.1126/sciadv.ade7702